MSG MPEF Reprocessed CDR Validation Report

Doc.No.	:	EUM/OPS/REP/14/761588
Issue	:	v3A
Date	:	11 March 2015
WBS	:	

EUMETSAT
Eumetsat-Allee 1, D-64295 Darmstadt, Germany
Tel: +49 6151 807-7
Fax: +49 6151 807 555
http://www.eumetsat.int

Document Change Record

Issue / Revision	Date	DCN. No	Changed Pages / Paragraphs
V1-V2E	25/06/2014		Initial working versions
V2F	12/01/2015		Final published version
V3A	11/03/2015		Final version after DRR meeting

Table of Contents

1 INTRODUCTION

1.1 Purpose and scope

This document is the validation report for the Meteosat Second Generation (MSG) reprocessed dataset Release 1. The reprocessing period covers March 2004 to December 2012. This validation has been performed internally at EUMETSAT. The reprocessed products that are validated are the Atmospheric Motion Vectors (AMV), the Clear Sky Radiance (CSR), and the All Sky Radiance (ASR).

The validation procedure that was performed is as comprehensive as possible. Inherent to this validation is that not always an independent dataset exists to validate the MSG products. Such products have been operational at EUMETSAT since 2004 but no real long-term validation has ever been performed for the products included in this report. This validation performed mainly ensures a full sanity check of the mentioned reprocessed products and in particular their stability in time. It is expected that the reprocessed MSG dataset will be valuable for climate studies given their high temporal stability.

1.2 Document structure

Section	*Contents*
Section 1	This introduction
Section 2	AMV validation
Section 3	CSR validation
Section 4	ASR validation
Section 5	Summary and conclusions

1.3 Applicable documents

Number	*Document Name*	*EUMETSAT Reference Number*
AD1	Climate Service Development Plan	EUM/C/82/14/DOC/28

1.4 Reference documents

Number	*Document Name*	*EUMETSAT Reference Number*
RD1	MSG R-MPEF Products User Manual: Collection 1	EUM/USC/MAN/14/755825
RD2	MSG Meteorological Products Extraction Facility Algorithm Specification Document	EUM/MSG/SPE/022
RD3	Verification plan and test results RMPEF MSG	EUM/OPS/TEN/11/695816

1.5 Background

A new global reanalysis, ERA-5, covering the satellite era will be produced by the European Centre for Medium-Range Weather Forecasts (ECMWF) to replace the existing ERA-Interim reanalysis. The European Union Framework 7 project ERA-CLIM (http://www.era-clim.eu) has developed observational datasets suitable for global climate studies, with a focus on the past 100 years. These datasets include atmospheric, oceanic, and terrestrial observations from a variety of sources, high-resolution global reanalysis products of the observations, and associated data quality information needed for climate applications.

In the framework of the ERA-CLIM project, EUMETSAT has reprocessed several Climate Data Records (CDRs) using level 1.5 images acquired by the Spinning Enhanced Visible and Infrared Imager (SEVIRI) instrument onboard the geostationary Meteosat Second Generation (MSG) satellites with the aim to provide the data for assimilation into the new ECMWF reanalysis. This first reprocessing of SEVIRI derived operational products covers the period 2004-2012. Three-hourly Atmospheric Motion Vectors (AMVs), Clear Sky and All Sky Radiances (CSR and ASR) were generated using the latest operational Meteorological Product Extraction Facility (MPEF) algorithms [RD2] (Version 1.5.3, 2013) available at the time of the reprocessing and the ERA interim data as a forecast input (***Figure 1)***. The forecast data are used for the radiative transfer calculaltions. Those CDRs are available and can be requested from the EUMETSAT Data Centre.

This validation report presents an analysis of the time series of the reprocessed MPEF products that provides insight into their temporal consistency and possible issues with the data record. The products included in this report are the AMV, the CSR, and the ASR products. Those products were delivered as part as of the ERA-CLIM project.

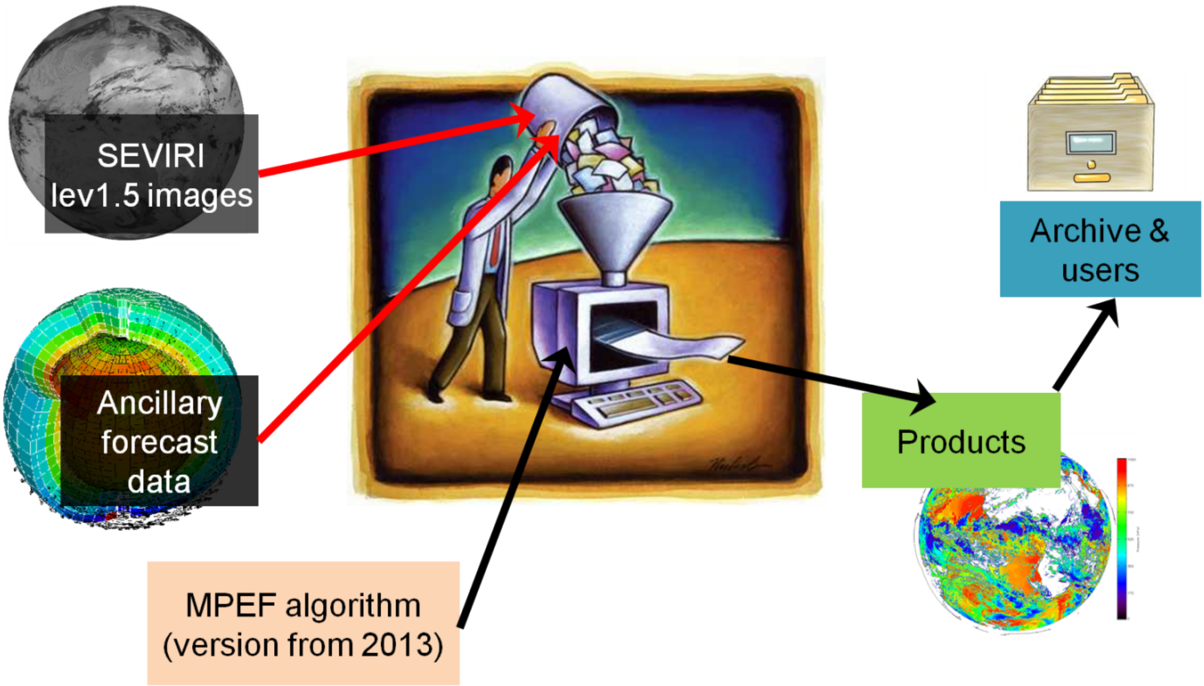

Figure 1: *Schematic of the Reprocessing Meteorological Product Extraction Facility (RMPEF).*

1.6 The Evaluation strategy

The reprocessed MSG data record relies on the latest algorithms available at the time of the reprocessing (Version 1.5.3, 2013). Our validation of the reprocessed MSG SEVIRI products has been conducted internally at EUMETSAT. The approach has been

- to rule out any major reprocessing issue,
- to test the stability of the dataset, and
- to perform a validation against external datasets depending on their availability and our resources.

Details about the reprocessing environment and the product format can be found in [RD1]. The RMPEF system verification can be found in [RD3]. The latter also contains the link between the reprocessed and corresponding near real-time products. Because the comparison between these two datasets has shown a great similarity, the MPEF algorithm descriptions in [RD2] can be considered as a substitute for the Algorithm Theoretical Basis Document (ATBD) for the RMPEF Release 1 dataset.

1.7 Reprocessed products

A subset of the MPEF operational products have been reprocessed for the entire MSG period from April 2004 until December 2012 and archived in the EUMETSAT archive. The following sections present detailed validation of the reprocessed products.

1.8 Definitions of statistical measures

The statistical parameters used in this report, mainly used for the AMV products, are the following:

- NC is the number of collocations between reference observation vectors [u_r,v_r]) and all the corresponding MSG vectors [u,v];
- SPD is the mean wind speed. Note that the wind speed can be decomposed in its zonal (u) and meridional (v) components

$$SPD = \sqrt{u^2 + v^2};$$

- BIAS is the difference between the mean satellite wind speed and the mean reference speed;

$$BIAS = \frac{1}{NC}\sum_{i=1}^{NC}\left(\left(\sqrt{u_i^2 + v_i^2}\right) - \left(\sqrt{u_r^2 + v_r^2}\right)\right)$$

- MVD is the mean vector difference

$$MVD = \frac{1}{NC}\sum_{i=1}^{NC} VD_i$$

where $VD_i = \sqrt{(u_i - u_r)^2 + (v_i - v_r)^2}$

- RMSE is the root-mean-square error (RMSE) traditionally reported as the square root of the sum of the squares of the mean vector difference and the standard deviation about the mean vector difference

$$RMSE = \sqrt{(MVD)^2 + (SD)^2}$$

$$SD = \sqrt{\frac{1}{NC}\sum_{i=1}^{NC}\left(VD_i - MVD\right)^2}$$

- CC is the correlation coefficient computed as the linear Pearson correlation coefficient, where the value CC = 1 means a perfect positive correlation and the value CC = -1 means a perfect negative correlation. x and y are the SPD of the observed wind (MSG) and the reference, respectively.

$$CC = \frac{\sum_i (x_i - \bar{x})(y_i - \bar{y})}{\sqrt{\sum_i (x_i - \bar{x})^2}\sqrt{\sum_i (y_i - \bar{y})^2}}$$

The normalized parameters that will be independent of the magnitude of the wind vector are defined as:

- Normalized bias: $NBIAS = {}^{BIAS}/_{SPD}$
- Normalized mean vector difference: $NMVD = {}^{MVD}/_{SPD}$
- Normalized root-mean square error: $NRMSE = RMSE/SPD$

2 ATMOSPHERIC MOTION VECTORS

2.1 Product definition

Each atmospheric wind vector is represented by its speed (m/s), direction (°) as shown in

Figure 2, and height (given in hPa). The final hourly wind product is an average of three intermediate products derived every 15 minutes. Each wind vector is accompanied by a quality index as defined in *Holmlund et al., 2001*. The quality index takes into account the consistency between the three intermediate vectors and the consistency with the surrounding vectors. See [RD2] for more details. For time reprocessing constraints, the winds were only derived every three hours.

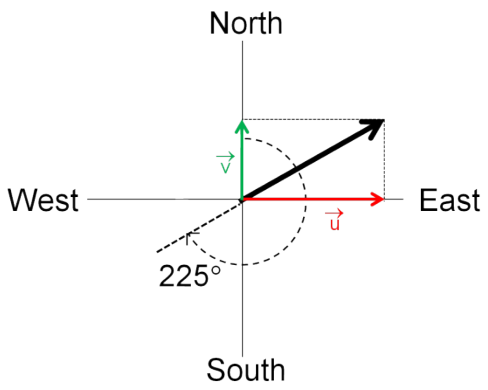

Figure 2: *Wind direction measured in degrees in clockwise direction starting from the north. For example a direction of 225° represents a wind blowing from the south west. The altitude of the wind is expressed in hPa.*

2.2 Comparison with operational products

The near real time (NRT) operational AMV production at EUMETSAT is continuously monitored (*Carranza et al., 2012*). One parameter monitored is the number of wind vectors produced per hour. The scientific development of the AMV retrieval algorithm and changes in operations over time has led to abrupt changes in the number of retrieved winds. In mid 2005, a change in the height assignment method was introduced leading to a 20% decrease in the number of produced AMVs. At the time Meteosat-9 became the operational satellite in April 2007, the number of AMVs increased by ~18%. This was due to the extension of the geographic processing area. The number of produced AMVs has also varied due to a few more minor algorithm changes (*Carranza et al., 2012*). The last big change in the height assignment method was introduced in September 2012 (*Borde et al., 2014*). It has led to an increase of a further 10 % in the number of AMVs. Figure 3 shows the variation in the number of operational and reprocessed AMVs over the reprocessed period. The disruptive nature of the blue curve makes immediately clear that an assessment of climate variability at inter-annual or longer time scales is very difficult/impossible using the operational NRT AMV products retrieved from the current EUMETSAT archive. When the same AMV algorithm is used for the entire eight year period (2004-2012), the number of winds remains stable at around 10000 winds produced per hour in the IR channel. This example clearly illustrates the benefit of the reprocessing activity.

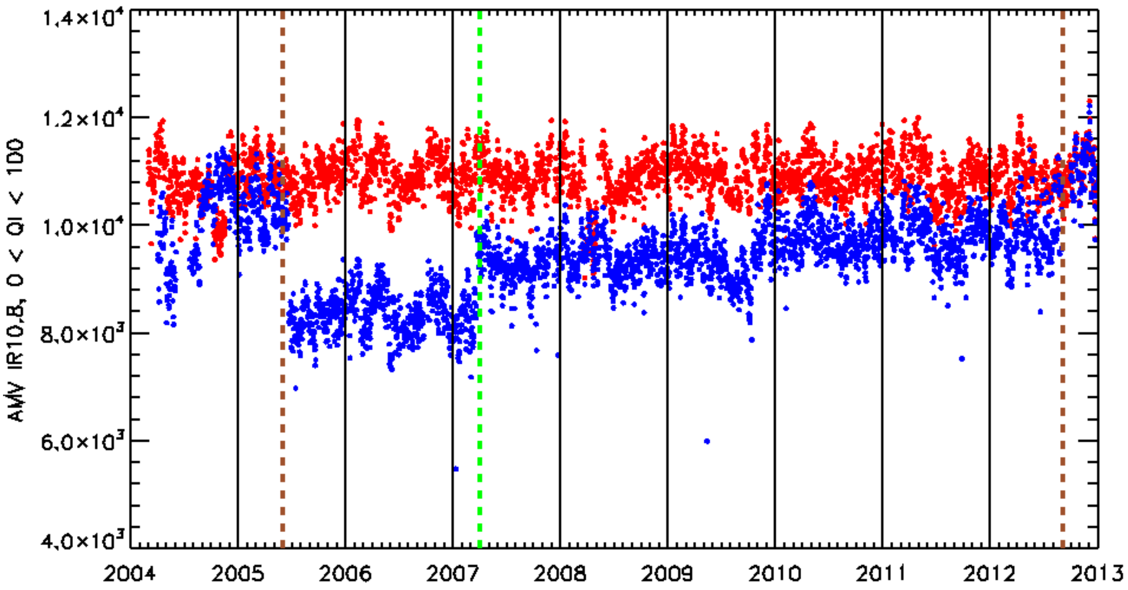

Figure 3: *Number of hourly derived AMVs in the IR10.8 channel. Blue dots are the number of AMVs extracted operationally and stored in the MPEF database. Red dots are the number of reprocessed AMVs for the corresponding slots. The main changes in the algorithms are represented by the brown dashed lines; the changes in satellite are represented by the green dashed line. The benefit of the reprocessing is clear.*

2.3 Temporal stability

The wind speed and height (given in pressure units) were zonally averaged (Figure 5) over the entire 8-year period as well as the zonal and meridional components of the wind vectors (Figure 4). The height of the wind vector depends on the cloud analysis (CLA) results see *RD2* and *Hamann et al., 2014* for more details on the CLA derivation. The series appears stable over the whole 8-year period with a recurring annual variability in average speed distribution clearly visible in the northern subtropics. The relatively slow tropical easterlies (or tradewinds) can be observed around the equator and the stronger westerlies north and south of 30°N and 30°S. The movement of the Inter Tropical Convergence Zone (ITCZ) is clearly in the northern hemisphere with the intrusion of easterlies on the northern hemisphere on a yearly cycle associated with the displacement of the meteorological equator. The wind height varies seasonally with higher winds (in altitude) close to the equator and lower winds around 30° latitude in both hemispheres. The winds exhibit the same stable behaviour in all SEVIRI channels. The change of satellites in 2007 is invisible.

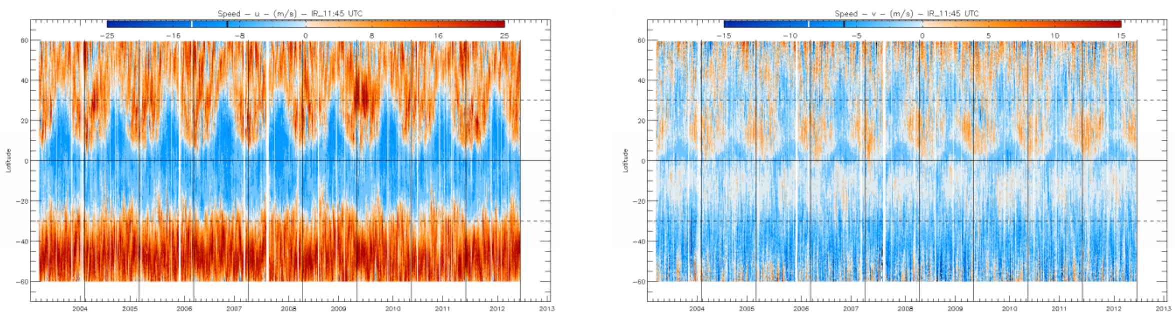

Figure 4: *Zonal (left) and meridional component (right) of the zonally-averaged AMVs for the period 2004-2012 at 11:45 UTC for channel IR108. Note that the white vertical lines correspond to short data outages.*

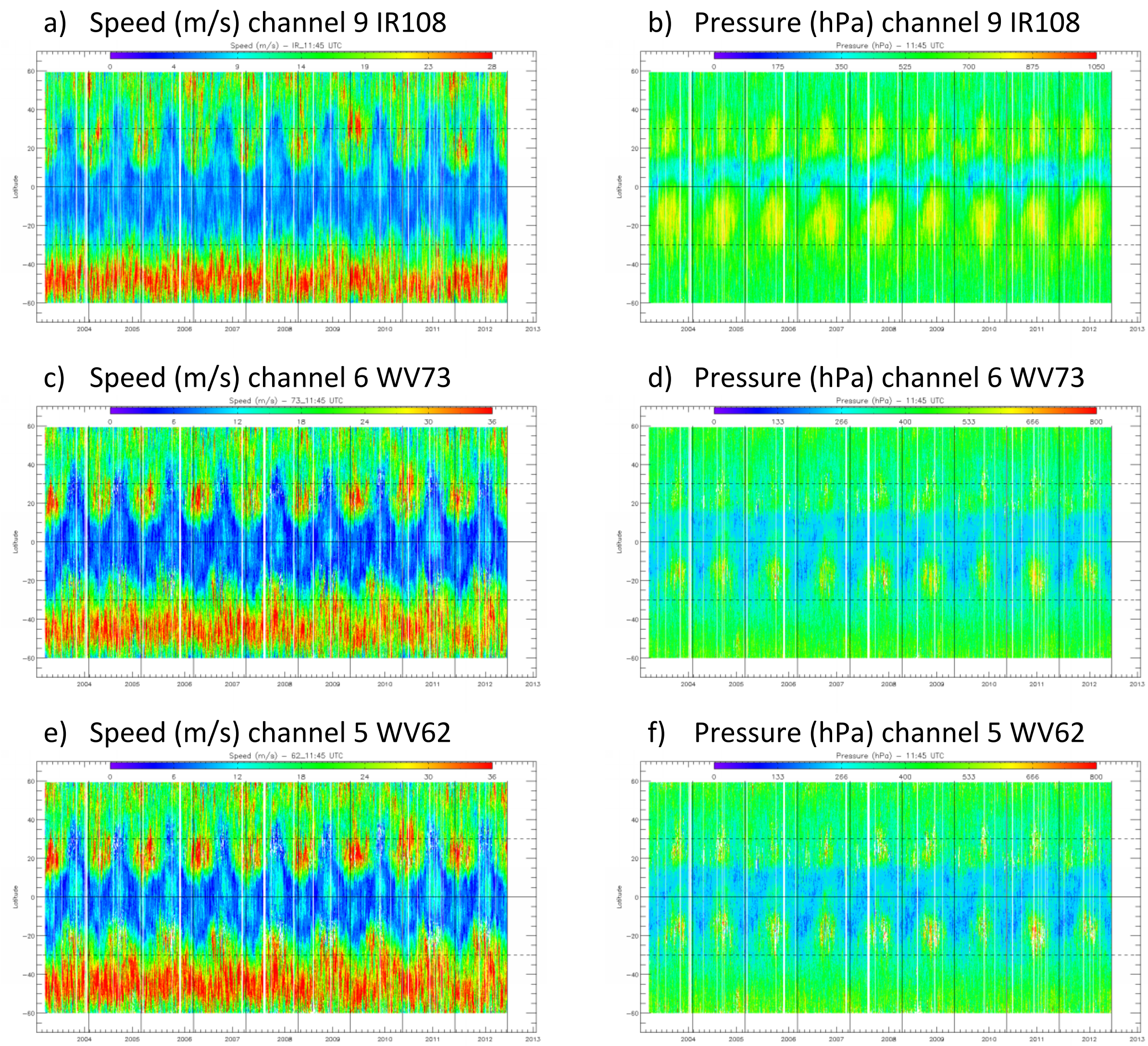

Figure 5: *Speed (in m/s) and altitude (in hPa) of the zonally-averaged AMVs for the period 2004-2012 at 11:45UTC for channel IR108 (10.8 µm), WV73 (7.3 µm), and WV62 (6.2 µm). Note that the white vertical lines correspond to short data outages.*

Figure 6 shows the annual averaged wind speed and the height of the IR winds for 2006. An area of low levels winds is located over the southern Atlantic ocean whereas high level winds are blowing over the tropics and the African continent. Strong wind speed areas are present polewards of 30°. Analysing the year 2006, it can be noticed that the annual cycle of the wind speed is seen in several atmospheric layers (Figure 7). Low, mid and high levels winds exhibit the same annual cycle for the speed. The winds located the highest in altitude are the fastest especially over the southern ocean south of 35°S with wind speeds over 25 m/s, a region known as the “Roaring Forties”. The latitude ranges for the Roaring Forties is shifting towards the South Pole in the northern winter, and towards the Equator in the northern summer. Over the equatorial region, the wind speed is lower at about 10 m/s. Low level winds are slow with an average below 9 m/s.

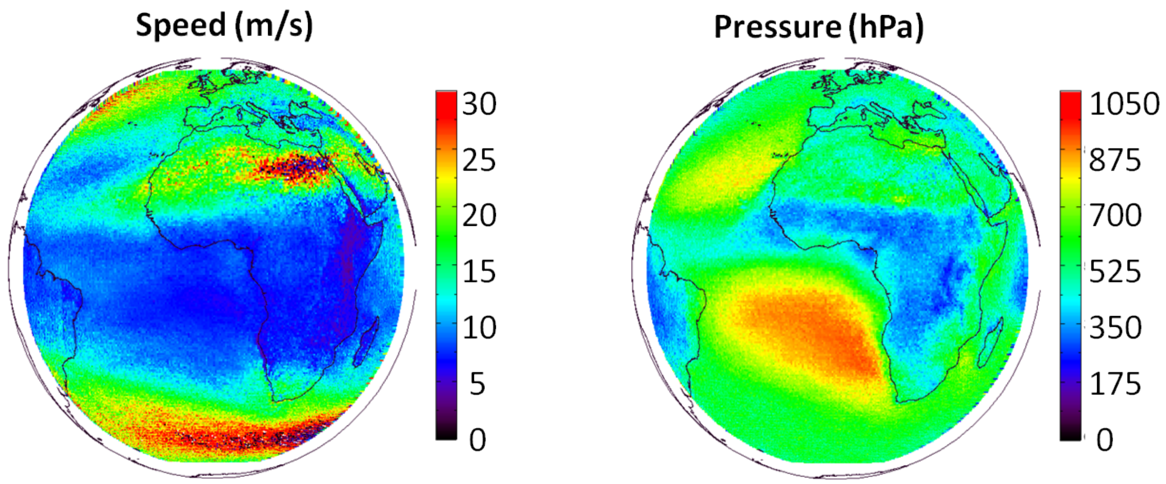

Figure 6: *AMV speed and altitude (represented in pressure) (IR108 channel) averaged for the year 2006 at 11:45UTC.*

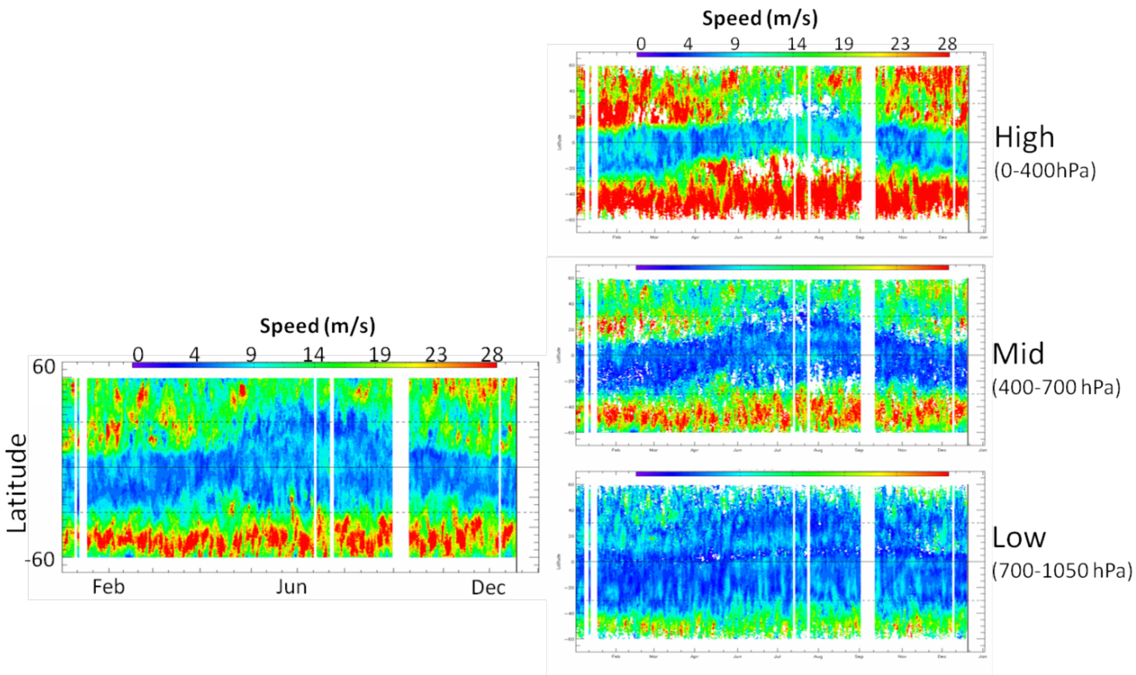

Figure 7: *Zonally-averaged AMV speed for the year 2006 at 11:45UTC for channel IR108 (10.8 µm). The column on the left shows all winds and column on the right shows the averaged speed of low, mid and high level winds.*

In conclusion the reprocessed AMVs are stable and exhibit geographical and seasonal features in line with well known atmospheric circulation patterns. Recurring annual variability in average speed distribution is clearly visible in the northern subtropics. Constantly high wind speeds (> 25 m/s) occur over the southern oceans (Roaring Forties).

2.4 Comparison with other datasets

2.4.1 Comparison with radiosonde observations

The statistical parameters used for the comparison are those proposed at the Third International Wind Workshop (Ascona, Switzerland, 1996) and recommended by the Coordination Group for Meteorological Satellites (CGMS) for the international comparison of satellite winds.

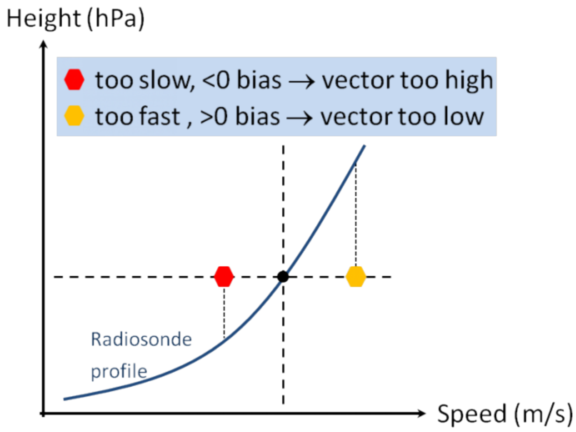

Figure 8: *Schematic of the bias between satellite wind and the observation. Generally, the speed increases with height. A negative bias (obs-sonde) can indicate that the satellite wind is too high compared to the observation.*

The MSG winds were collocated against radiosondes from the RAOBCORE (*Haimberger*, 2012) data record. For each RAOBCORE data record available, all MSG winds located within a 100 km maximum distance and with a maximum of 30 minutes acquisition time difference are retained for the comparison. Only MSG wind vectors with a final quality indicator (*Holmlund, 2001*) higher than 50 are considered. The QI threshold used for filtering AMVs is dependent on the user need. The threshold of 50 has been chosen to consider a broad number of winds collocations to be statistically representative. The number of available collocations depends directly on the amount of high-quality AMVs produced. Over the eight year period of 2004-2012, 751694 collocations of RAOBCORE and MSG winds within 30 minutes and 100 km were found. Most of the collocations are located over Europe and over land. There are no collocations over the ocean because no radiosonde observations were available (see Figure 9). When the maximum acquisition time difference between a radiosonde and a satellite wind is set to 90 minutes, about 30% more collocations are found, but the statistics remain essentially the same.

Both MSG satellite AMVs and radiosonde observations present the highest frequency of wind speed between 6 and 8 m/s. MSG derived slow winds (below 4 m/s) are more frequent than the corresponding radiosonde observed winds (see Figure 10).

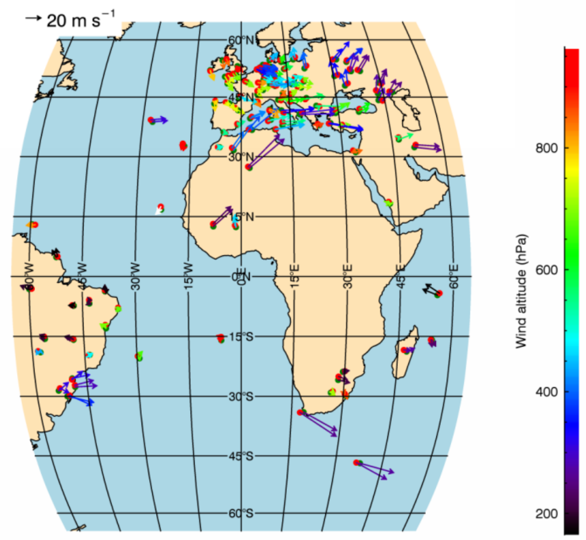

Figure 9: *Example of collocation of a radiosonde and MSG AMV for March 2006 at 12 UTC. Green and red circles indicate the positions of the radiosonde and the corresponding collocated satellite wind, respectively. The colour of the vector indicates its height in hPa.*

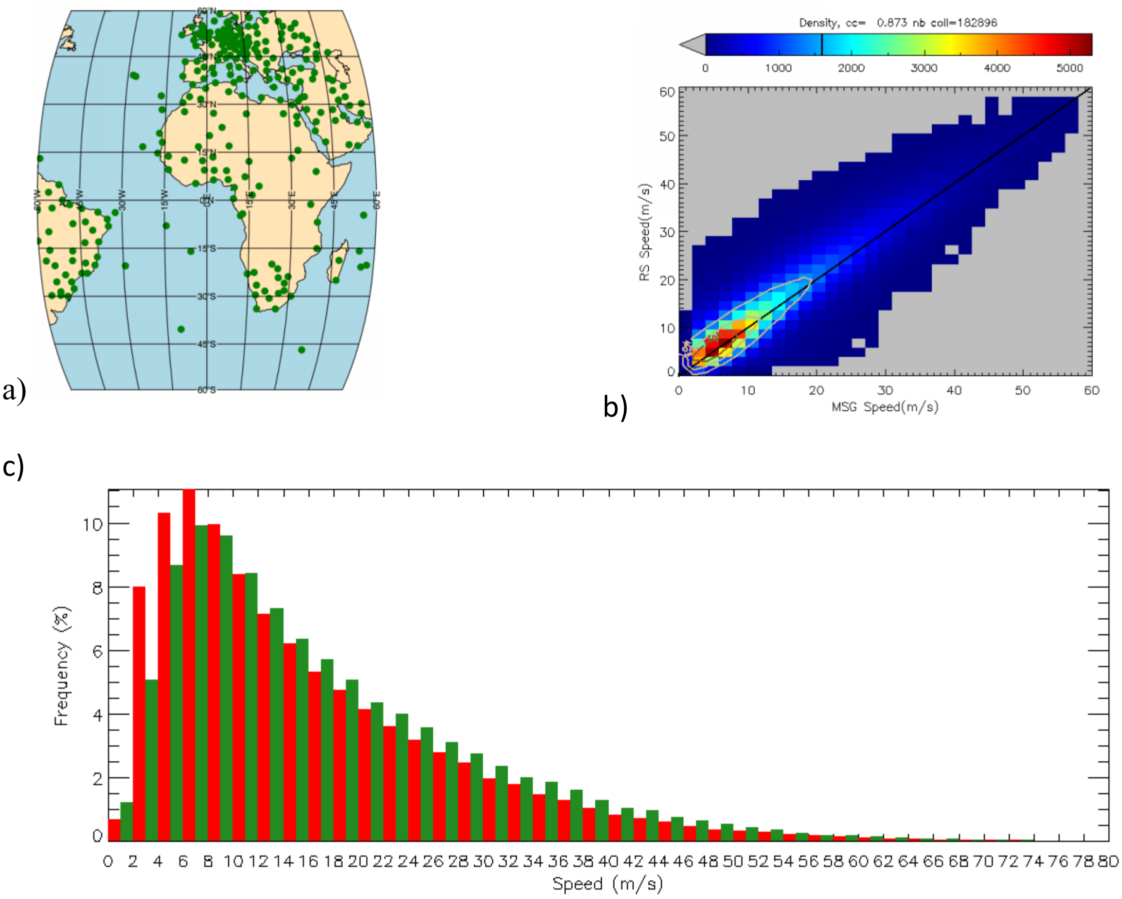

Figure 10: *Radiosondes observations collocated with MSG winds for the months of December, January and February 2004-2012 at 12 UTC. A total of 182912 collocations have been found for 270 individual radiosonde locations. a) Spatial distribution of the radiosonde locations, b) scatter plot of the speed, and c) speed frequency distribution, MSG is shown in red and RAOBCORE in green.*

Table 1 and Table 2 show the statistics split by wind height and by seasons. Similar statistics against radiosondes were done in the table 1 of *Borde et al. 2014*. The conclusion of this study was that using the wind algorithm used in this reprocessing exercise (CCC method), the statistics regarding the bias and RMS show a general positive or neutral overall impact for all channels using the, especially for high-level and midlevel winds compared with the previous wind algorithm used at EUMETSAT. The comparison with radiosondes observations over the entire MSG period show the half of the collocations are found for high level AMVs. The four seasons exhibit similar statistics. For the infrared channel, the speed bias is always negative and never above 2 m/s. The MSG derived winds are slower than the radiosonde observation. On averaged MSG winds are about 6m/s slower. The bias is less for low level wind. The higher level winds are faster than the lower level winds and have the highest speed bias. For the water vapour channel the bias is overall positive but only high level winds should be considered and they exhibit as for IR channel a negative bias.

		DJF				JJA			
		All	low	mid	high	All	low	mid	High
NC	IR108	182896	39909	52118	90921	183488	44237	57293	81995
	WV73	173679		62520	104238	158351		53970	96732
	WV62	137739			97949	117823			84836
	VIS	51547	51547			47947	47947		
SPD (m/s)	IR108	17.30	8.52	15.46	22.17	14.11	7.85	12.27	18.77
	WV73	19.29		15.53	22.23	16.25		12.60	18.89
	WV62	20.21			20.93	17.25			19.27
	VIS	8.55	8.55			7.86	7.86		
BIAS (m/s)	IR108	-1.54	-0.6	-1.44	-2.00	-1.17	-0.30	-1.18	-1.61
	WV73	0.001		1.07	-0.97	0.32		1.48	-0.58
	WV62	1.29			-0.006	1.51			-0.07
	VIS	-1.06	-1.06			-0.76	-0.76		
NBIAS (m/s)	IR108	-0.09	-0.07	-0.09	-0.09	-0.08	-0.04	-0.10	-0.09
	WV73	0.00		0.07	-0.04	0.02		0.12	-0.03
	WV62	0.06			-0.0003	0.09			0.003
	VIS	-0.12	-0.12			-0.09	-0.09		
MVD (m/s)	IR108	5.77	4.42	6.04	6.21	5.20	4.14	4.99	5.92
	WV73	6.69		7.35	6.02	6.15		6.42	5.82
	WV62	7.46			5.94	7.15			5.98
	VIS	3.76	3.76			3.80	3.80		
NMVD (m/s)	IR108	0.33	0.51	0.39	0.28	0.37	0.53	0.41	0.31
	WV73	0.35		0.47	0.27	0.38		0.51	0.31
	WV62	0.37			0.28	0.41			0.31
	VIS	0.44	0.44			0.48	0.48		
RMSE (m/s)	IR108	7.76	6.36	7.93	8.21	6.94	5.70	6.44	7.83
	WV73	9.08		9.88	7.93	8.36		8.74	7.71
	WV62	10.19			7.85	9.67			7.92
	VIS	4.72	4.72			4.85	4.85		
NRMSE (m/s)	IR108	0.45	0.75	0.51	0.37	*0.49*	0.73	0.52	0.42
	WV73	0.47		0.64	0.36	*0.51*		0.69	0.41
	WV62	0.50			0.37	*0.56*			0.41
	VIS	0.55	0.55			*0.62*	0.62		
SD (m/s)	IR108	5.18	4.57	5.15	5.36	4.60	3.92	4.06	5.13
	WV73	6.13		6.61	5.16	5.66		5.93	5.05
	WV62	6.93			5.11	6.51			5.19
	VIS	2.87	2.87			3.00	3.00		
Correlation coefficient	IR108	0.87	0.55	0.76	0.89	0.85	0.57	0.75	0.86
	WV73	0.83		0.68	0.90	0.81		0.68	0.87
	WV62	0.81			0.89	0.78			0.87
	VIS	0.72	0.72			0.66	0.66		

Table 1: *Statistical parameters obtained for collocated RAOBCORE and MSG wind vectors. All, low (700 ≤ P ≤ 1050 hPa), mid (400 ≤ P ≤ 700 hPa), and high (0 ≤ P ≤ 400 hPa) MSG winds with a QI greater than 50 acquired within 30 minutes and 100 km of a radiosonde are considered (NC) for the month of December, January, and February (DJF) and June, July, and August (JJA) for the years 2004-2012. For the WV channels, the low level AMVs should not be considered neither the WV6.2 mid level winds because those winds are artificially considered as cloudy winds (due to CLA cloud type) but they should be considered as clear sky WV winds.*

	MAM				SON			
	all	Low	mid	high	all	Low	mid	high
NC	194369	35364	56756	102292	190941	44872	51926	94201
SPD (m/s)	16.02	8.11	13.72	20.02	15.79	8.30	13.59	20.57
BIAS (m/s)	-1.54	-0.60	-1.61	-1.81	-1.26	-0.59	-1.09	-1.67
NBIAS (m/s)	-0.10	-0.07	-0.12	-0.09	-0.08	-0.07	-0.08	-0.08
MVD (m/s)	5.45	4.21	5.56	5.81	5.36	4.04	5.44	5.94
NMVD (m/s)	0.34	0.52	0.41	0.29	0.34	0.48	0.40	0.29
RMSE (m/s)	7.29	5.97	7.32	7.67	7.15	5.46	7.06	7.88
NRMSE (m/s)	0.45	0.74	0.53	0.38	0.45	0.66	0.51	0.38
SD (m/s)	4.85	4.23	4.76	5.01	4.74	3.68	4.49	5.18
CC	0.87	0.57	0.75	0.88	0.87	0.62	0.76	0.87

Table 2: *As for Table 1 but for the month of March, April, and May (MAM) and September, October, and November (SON) for the years 2004-2012 and for the channel IR108.*

2.4.2 Comparison with GOES reprocessed AMVs

This section illustrates a similar behaviour of SEVIRI and GOES AMV in their overlap region. This comparison has exemplary character and is not performed over the entire period but only for the months of June and December 2008.

The Cooperative Institute for Meteorological Satellite Studies (CIMSS) institute has reprocessed GOES winds from 1995 until mid 2013 using the operational GOES-East and GOES-West satellites (GOES-8 to GOES-15). Hourly winds were derived from IR (10.7µm), WV (6.5µm), SWIR (3.9 µm) and Visible channels. This dataset can be found at: ftp://ftp.ssec.wisc.edu/velden/winds/wind_files/.

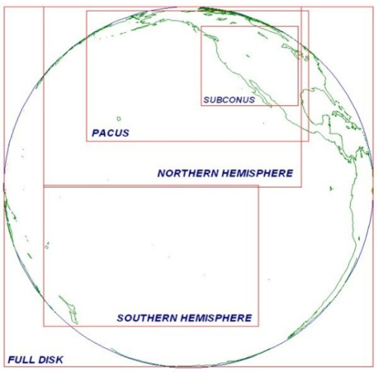

a) GOES WEST scanning metrics

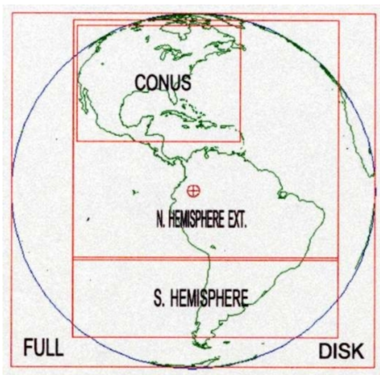

b) GOES EAST scanning metrics

For this AMV comparison, we have merged GOES reprocessed data with MSG. Both AMV products were re-gridded on a 0.5x0.5 regular grid. Only GOES East winds present overlap with MSG winds.

	11 UTC		20UTC	
	June	December	June	December

NC	822	8340	498	7552
GOES SPD	11.29	13.96	10.35	13.91
BIAS	-0.32	-0.44	-0.3	-0.43
NBIAS	-0.03	-0.03	-0.03	-0.03
MVD	2.07	2.49	2.21	2.67
NMVD	0.18	0.18	0.21	0.19
RMSE	3.18	3.95	3.25	3.88
NRMSE	0.28	0.28	0.31	0.28
SD	2.42	3.05	2.38	2.82
CC	0.94	0.94	0.90	0.94

Table 3: *Statistics for the months of June and December 2008 at 11UTC and 20UTC between MSG and GOES AMVs retrieved for the IR channel (bias = MSG – GOES).*

The overlap area is [60°W, 20°W], which includes relatively large viewing angles for the SEVIRI instrument. As shown in Table 3, there is relatively high correlation coefficient indicating consistency at least in wind direction. The bias is negative as for radiosondes. On average GOES seems to retrieve faster winds than the MSG produced winds (by 2m/s). The MSG winds vectors are probably assigned higher in the atmosphere than the GOES wind vectors. The altitude of GOES winds appear underestimated or overestimated compared to the MSG wind (Figure 11a and d) depending on the wind pressure level. Each algorithm uses a different method for height assignment. The CIMSS algorithm uses Equivalent Black Body Temperature (EBBT), CO_2 pressure, cloud base and model adjustment for (*Niemann et al., 1997*). The EUMETSAT algorithm uses the CCC method (*Borde et al., 2014*). The NWP forecast used for height assignment also differs. Another difference between GOES and MSG winds are the spatial and the temporal sampling as GOES derives wind between images separated by 30 minutes and not 15 minutes *Garcia-Pereda and Borde (2014)* have discussed the potential difference on the wind speed of such a difference in sampling. However, over a month, the global map of MSG and GOES winds is consistent (see Figure 11a-c).

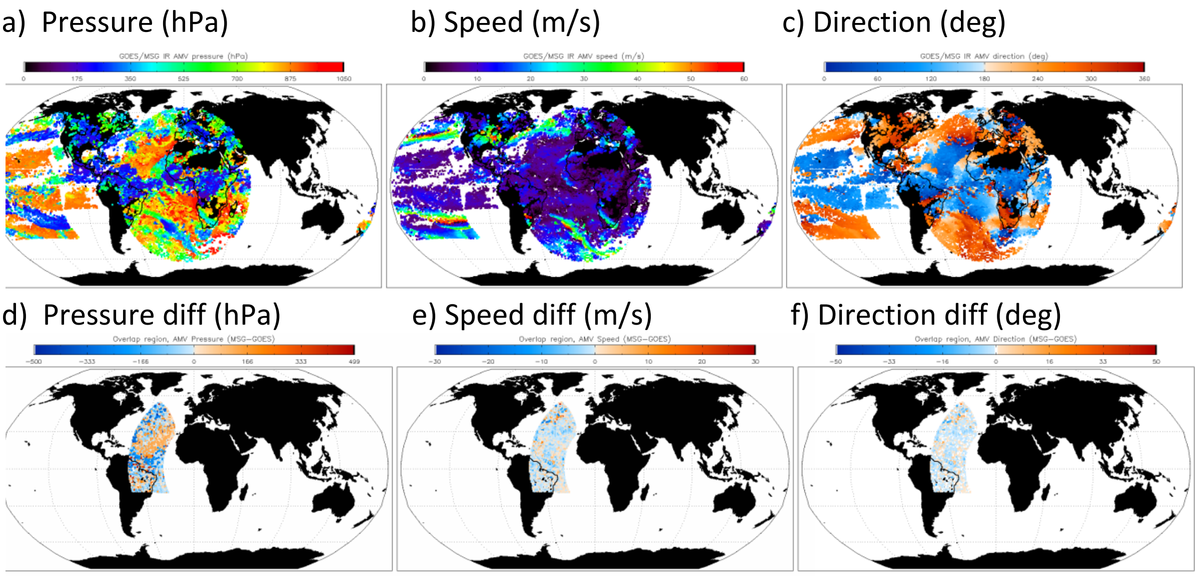

g) Pressure (hPa) h) Speed (m/s) i) Direction (deg)

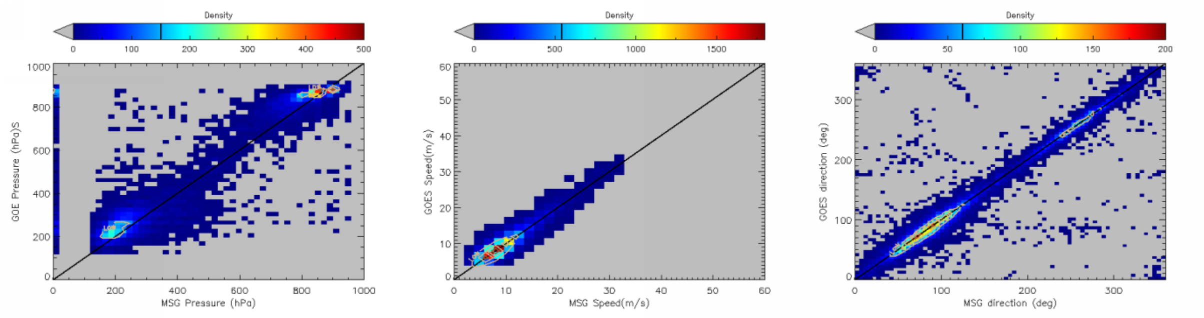

Figure 11: *Comparison between GOES and MSG AMVs for the month of June 2008. Top panels (a-b-c) present the winds for GOES and MSG on the 2nd of June 2008 at 12:45UTC, middle panels (d-e-f) present the difference in winds for the overlap region and bottom panels (g-h-i) present the scatter plot of GOES wind as a function of MSG wind for the month of June 2008. For each row, wind pressure, speed and direction are shown.*

In conclusion, the set of AMVs products provided to the ERA CLIM project from MSG and GOES data seem reasonably consistent.

2.4.3 An example of verification link between NAO and AMVs

To further verify the climatological validity of our products we analysed the winds derived in relation to positive and negative North Atlantic Oscillation (NAO) index phases.

The NAO index is defined as the difference of atmospheric pressure at sea level between Iceland and the Azores. The index (in northern hemispheric winter) indicates the strength and direction of westerly winds and the position of storm tracks across the North Atlantic and over Europe. Figure 12 shows respective AMVs over the North Atlantic Ocean for two extreme NAO conditions during 2010 (negative index) and 2011 (positive index). In a positive NAO phase, the westerly winds are strong while during a negative NAO index, westerly winds are almost suppressed. The reprocessed AMVs match quite well with the theoretical expectation of wind patterns for different NAO conditions. This gives confidence in the climatological quality of the retrieval. Only a few test cases on the correlation between NAO index and the reprocessed MSG AMVs have been done. There is certainly a need for further stronger work to be done to get better firm conclusions.

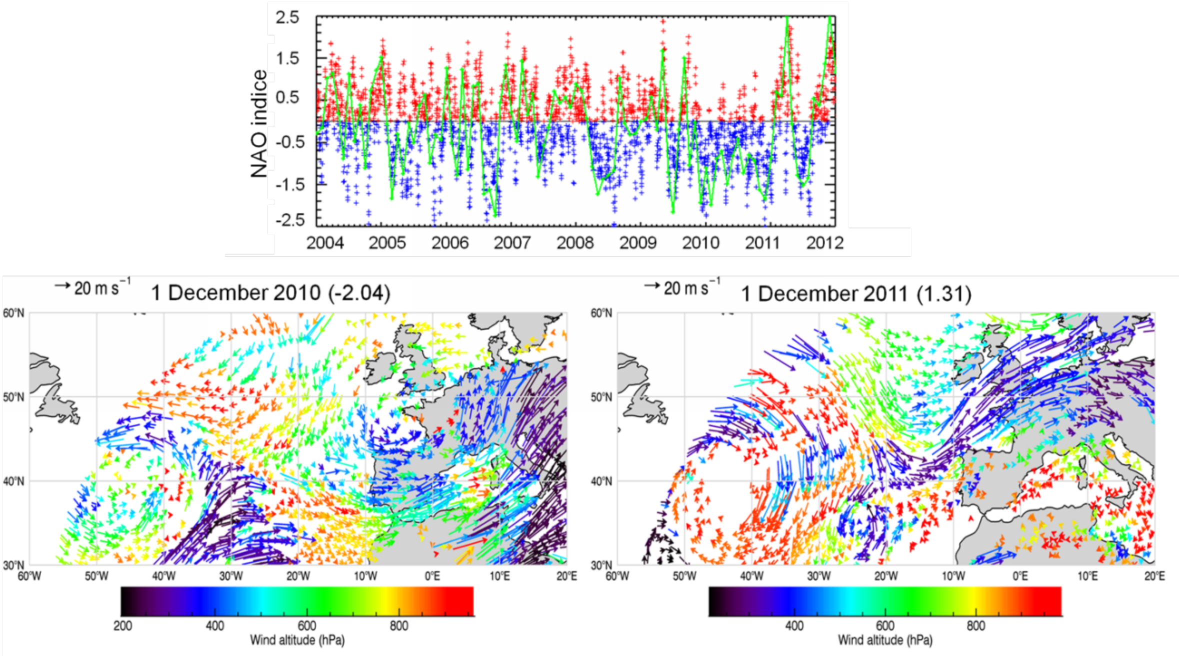

Figure 12: *An example of wind patterns under two different NAO conditions (bottom panels) for the 1st December 2010(NAO negative) and the 1st December 2011 (NAO positive). The top-right panel presents the time series of the daily NAO index in red and blue for positive and negative index, respectively as well as monthly NAO index in green. NAO data have been retrieved from https://climatedataguide.ucar.edu/climate-data/hurrell-north-atlantic-oscillation-nao-index-station-based (alternative version).*

2.5 Conclusion

Eight years of MSG AMVs were reprocessed. The AMV time series obtained is now homogeneous and stable over the period. The Global Climate Observing System (GCOS) requirements for upper-air winds retrieval are 2m/s at 20m/s, with 100hPa accuracy in height assignment (*GCOS, 2011*). The bias found with radiosondes and other satellite data is below 2m/s. The MSG wind speed is slower than radiosonde-observed winds by about 6m/s and than the GOES AMVs by about 2m/s.

3 CLEAR SKY RADIANCES

It is difficult to validate the reprocessed Clear Sky Radiance (CSR). CSR are very dependent on the cloud mask used and the cloud analysis product. The validation of the cloud product is not part of this report. Some information on the EUMETSAT Cloud Analysis product (CLA) can be found in [RD2] and its behaviour relative to other existing algorithm can be found in Hamann et al. (2014). The CSR products are used routinely at ECMWF since many years (Munro et al., 2004, Szyndel et al. 2005). The reprocessing in place at EUMETSAT relies on the same level 1.5 images that are used in the operational processing. The difference between the MPEF and the RMPEF CSR appears because different forecast data are used by the algorithm. The reprocessing uses ERA-Interim forecast data to avoid any temporal inconsistencies due changes in the ECMWF forecast model version. The forecast data are used for the radiative transfer calculations and have impact on the cloud detection and cloud height assignment results. The accuracy of the product depends mainly on the accuracy of the calibrated image data and the accuracy of the scenes analysis processing. This report focuses on the stability of the product over the 8-year period.

3.1 Product definition

The Clear Sky Radiances product contains information on mean brightness temperatures from regions that have been identified as clear sky, except for the WV channel where the CSR is also derived for areas containing low-level clouds. The CSR is retrieved using information at pixel level. The CSR product is generated hourly in the MPEF NRT processing, but has been reprocessed 3 hourly as the other RMPEF products. Even if the name of the product refers to radiances, only Brightness Temperatures (BT) are stored in the CSR product. MPEF [RD2] computes the CSR as an average of pixel brightness temperature in boxes of 16x16 pixels (about 50x50 km^2 at the sub satellite point (SSP) and 80x80 km^2 at 50° from the SSP). It also contains cloud coverage information, statistical and confidence information. In the current MPEF implementation, the pixel BTs are averaged inside 16x16 pixel boxes. It would be physically more correct to average the radiances in a box and then calculate the BT from this value. For homogeneity reasons, however, it has been decided to use the original MPEF algorithm also in the reprocessing.

3.2 Comparison with operational products

As no changes in the image calibration were done for this reprocessing, a check against the operational product is performed for a particular month only. The results are shown in Table 4. The bias between RMPEF and MPEF products is negligible (below 0.1K). This is probably because of compensating positive and negative biases in areas with low level clouds watched under different viewing angles. However, some slight differences appear mainly because of the cloud mask which is different due to the use of different forecast data. For the IR window channels, the RMPEF products are slightly warmer over the tropics (Figure 13). For the water vapour channels, the difference is more scattered over the entire product (Figure 14 and Figure 15). The spatial distribution of CSR brightness temperature over the month is quite similar between the RMPEF and MPEF products.

Channel	Average (K)	Std dev (K)	Bias (K)	Rms (K)
BT134	**269.40** (269.60)	**7.35** (6.94)	0.05	0.27
BT 12	**293.71** (293.88)	**11.19** (10.83)	0.07	0.47
BT 108	**295.40** (295.58)	**11.03** (10.62)	0.07	0.48
BT96	**268.45** (268.81)	**10.06** (9.32)	0.04	0.28
BT87	**292.51** (292.72)	**9.22** (8.72)	0.06	0.42
BT 73	**261.56** (261.66)	**6.66** (6.45)	0.016	0.13
BT 62	**241.71** (241.72)	**7.77** (7.75)	-0.00	0.09
BT 39	**297.35** (297.69)	**13.75** (13.37)	0.02	0.47

Table 4: *Statistics for the month of June 2008 at 11:45 UTC showing the differences between the RMPEF and the MPEF products. The average and the standard deviation are computed for the RMPEF or MPEF products when either one is defined but the bias and the rms are computed for RMPEF-MPEF when a valid retrieval is available for both of them. Bold and bracket values are reprocessed and operational values, respectively.*

BT10.8, June 2008 at 11:45

a) Monthly average of RMPEF CSR (K) and difference (K) of the average RMPEF-MPEF

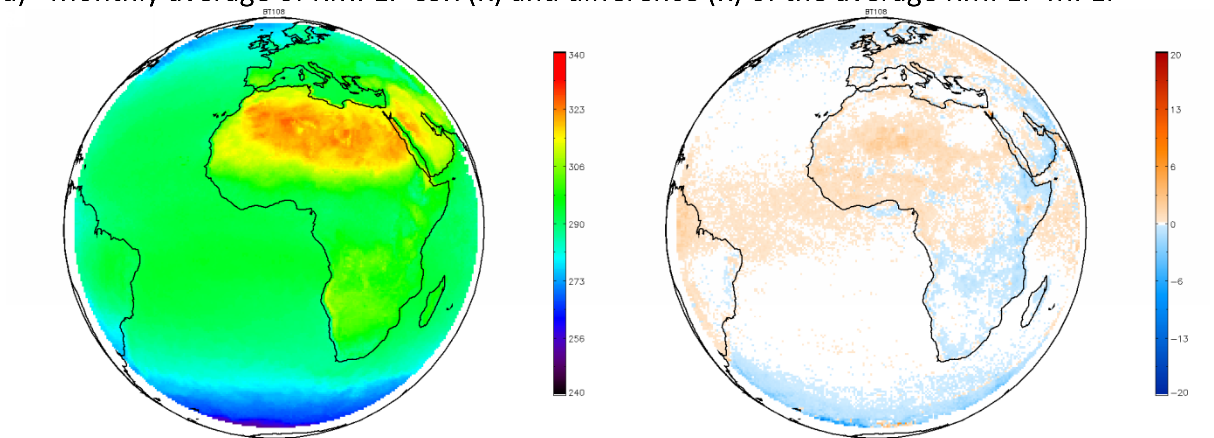

b)

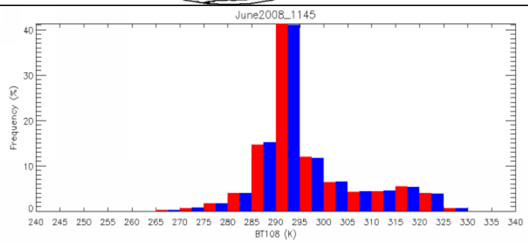

c)

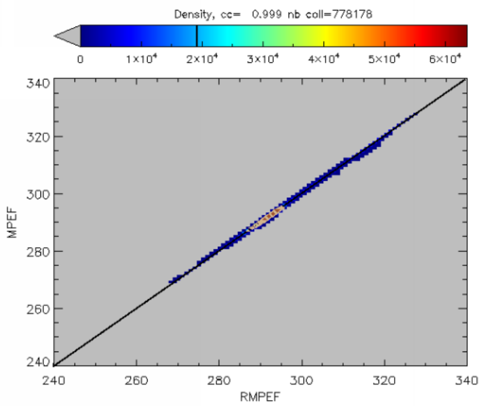

Figure 13: *a) Average of the RMPEF CSR BT for SEVIRI channel 10.8 µm and difference avg(RMPEF)-avg(MPEF), b) histogram of the RMPEF BT in red and the MPEF (in blue), and c) scatter plot of MPEF BT as a function of RMPEF CSR for the SEVIRI channel centred at 10.8 µm.*

BT7.3, June 2008 at 11:45

a) Monthly average of RMPEF CSR (K) and difference (K) of the average RMPEF-MPEF

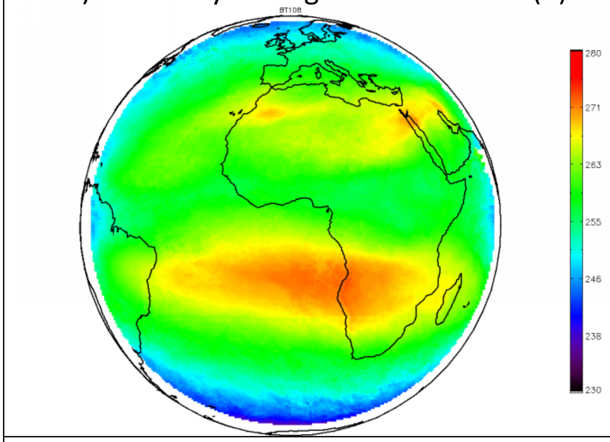

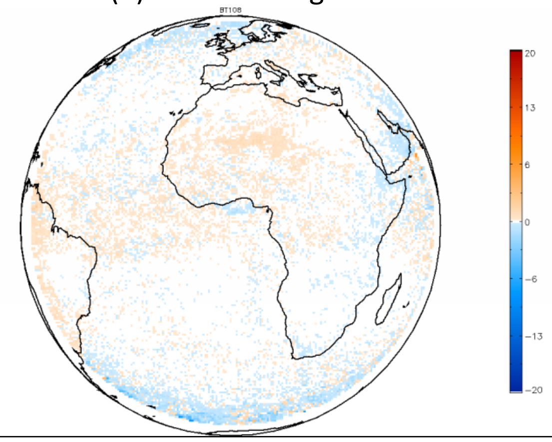

b)

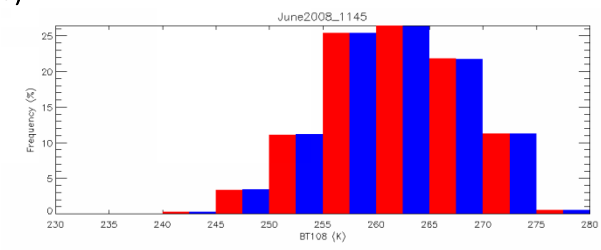

c)

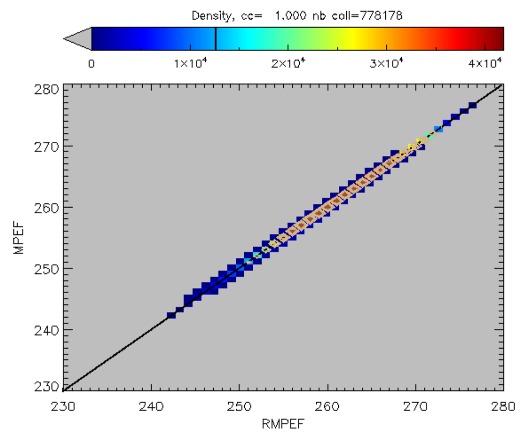

Figure 14: *Same as Figure 13 but for the SEVIRI channel centred at 7.3 μm.*

BT6.2, June 2008 at 11:45

a) Monthly average of RMPEF CSR (K) and difference (K) of the average RMPEF-MPEF

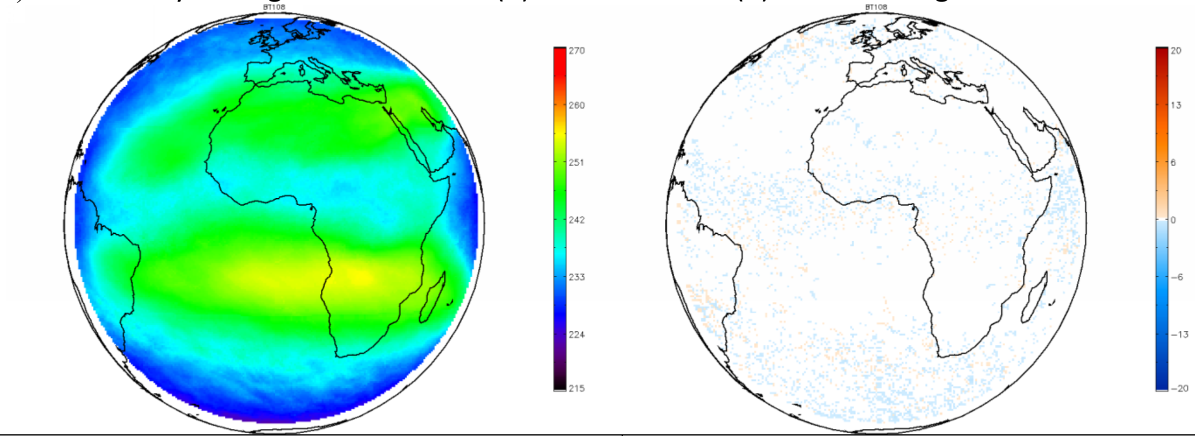

b)

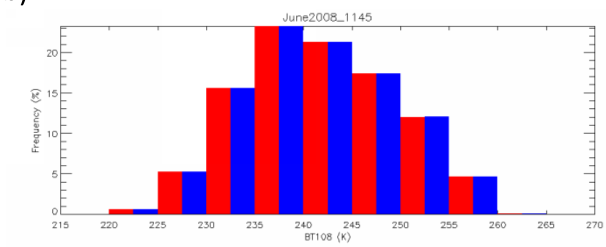

c)

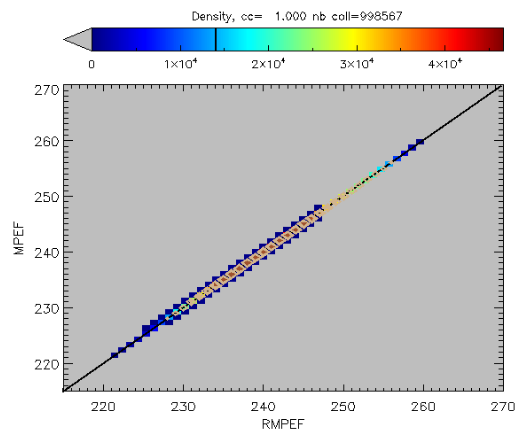

Figure 15: *Same as Figure 13 but for the SEVIRI channel centred at 6.2 µm.*

In conclusion, there are some differences between the RMPEF and MPEF CSR as expected. But the differences are very small, not significant and can be explained by the use of different forecast data.

3.3 Temporal stability

3.3.1 Global average

A time series of the mean clear sky brightness temperature has been produced at different time of the day as shown in Figure 16. It can be seen that the time series is very stable. The annual cycle is clearly seen following the known cloudiness seasonal cycle. The driver for the global CSR average is the northern part of Africa where deserts are located. The minimum of global averaged CSR is seen in winter (DJF) and the maximum appear in summer (JJA). The annual cycle is less clear at midday. The amplitude of the annual cycle is above 10 K and larger at 6 and 18 UTC than at midday and midnight where the amplitude of the annual cycle is about 7 K.

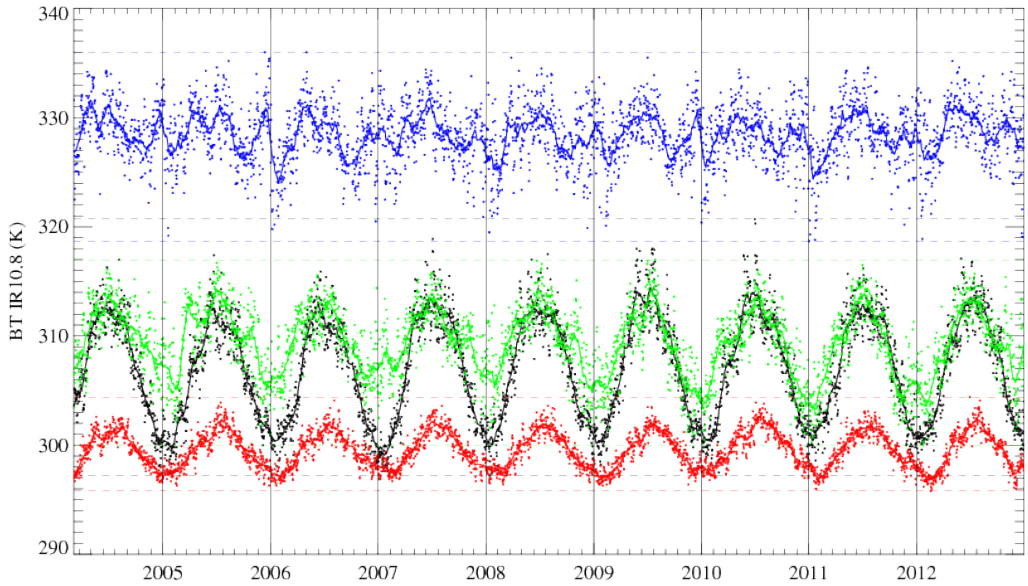

Figure 16: *Global average of the clear sky brightness temperature in channel 10.8 µm for the period 2004-2012 at 05:45, 11:45, 17:45 and 23:45 UTC represented in black, blue, green and red, respectively. The coloured lines are the running averages over 30 days while the dots are the daily measurement at a time.*

3.3.2 Zonal Average

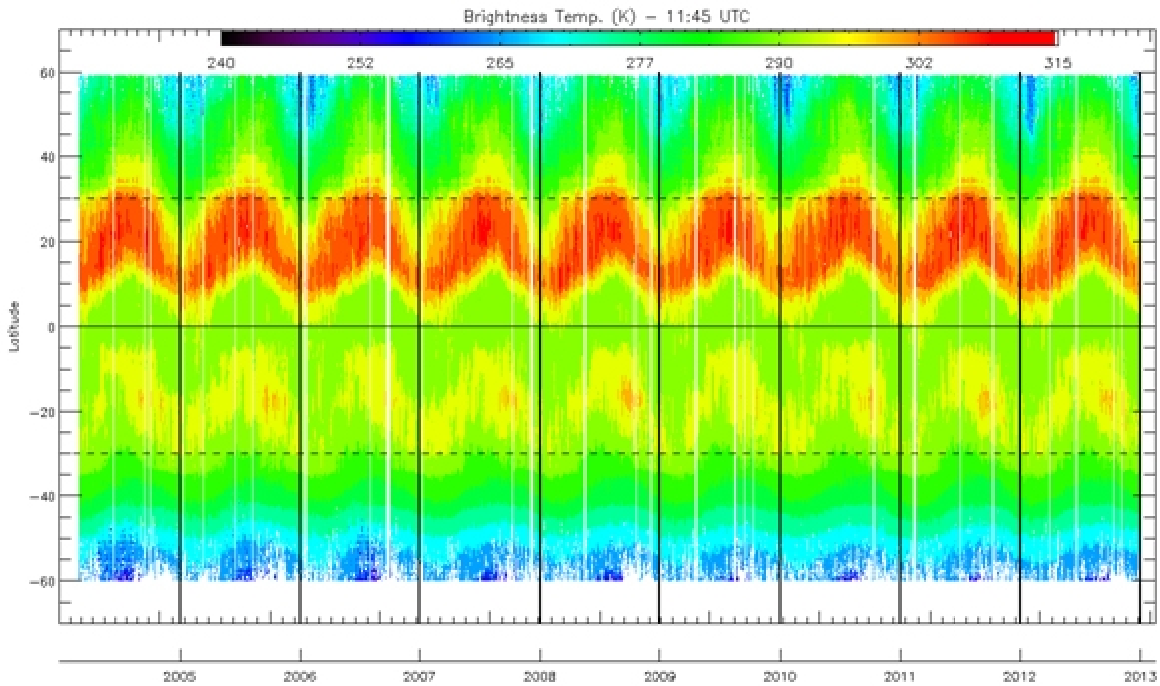

Figure 17*: Time series of CSR BT over the 8-year period 2004-2012 at 11:45 UTC for the SEVIRI channel 9 (10.8 µm).*

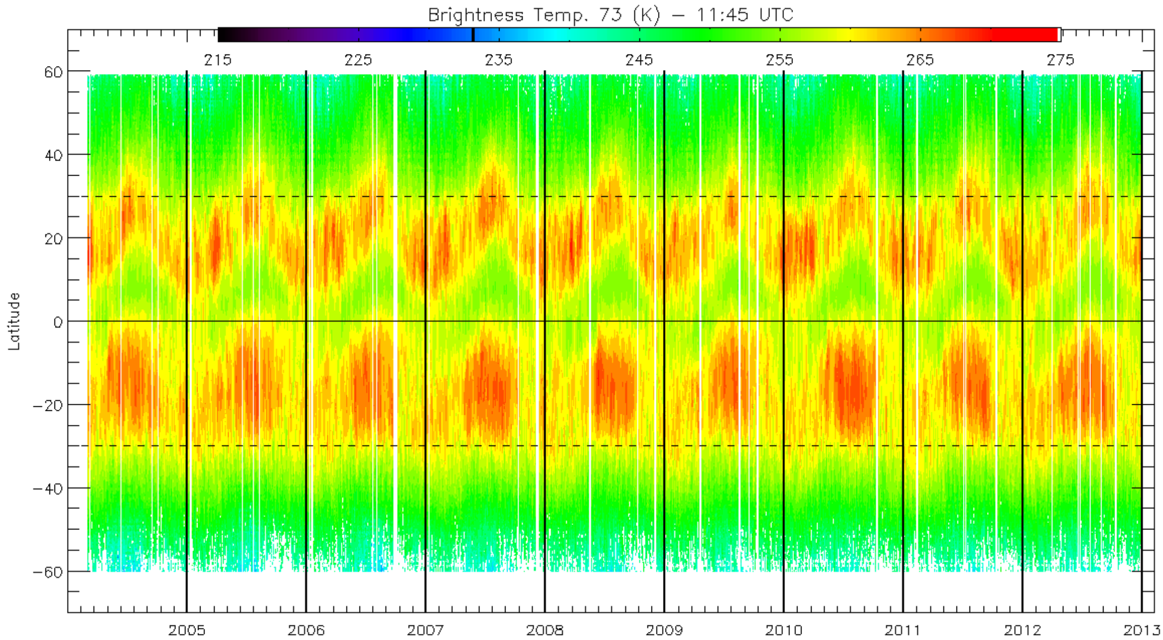

***Figure 18**: Time series of CSR BT over the 8-year period 2004-2012 at 11:45 UTC for the SEVIRI channel 6 (7.3 µm).*

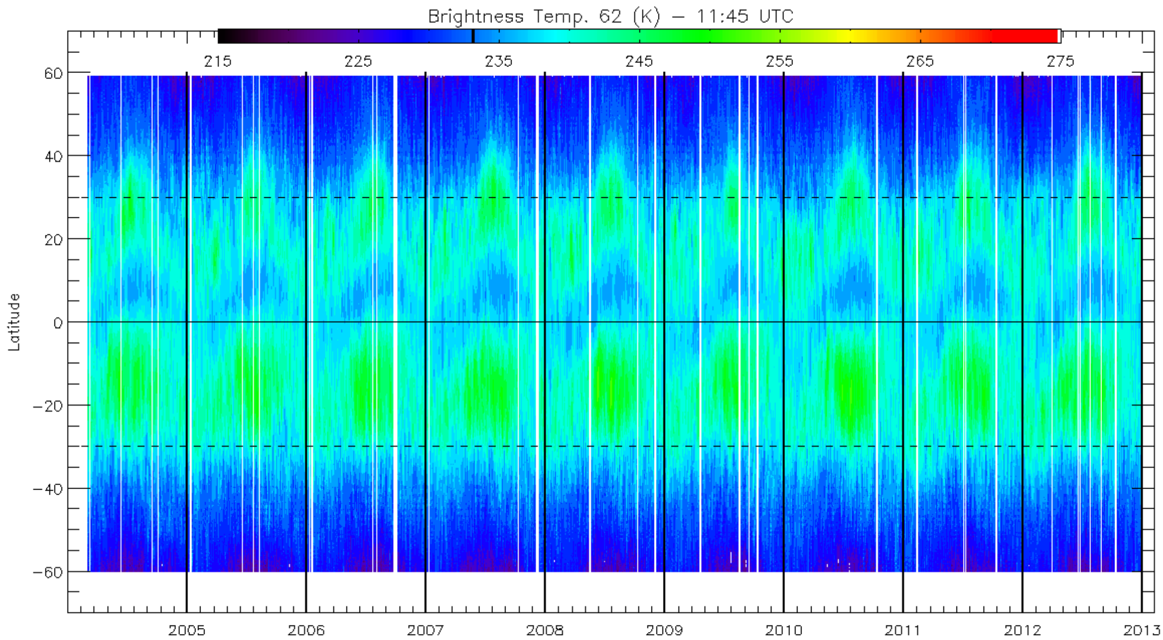

***Figure 19**: Time series of CSR BT over the 8-year period 2004-2012 at 11:45 UTC for the SEVIRI channel 5 (6.2 µm).*

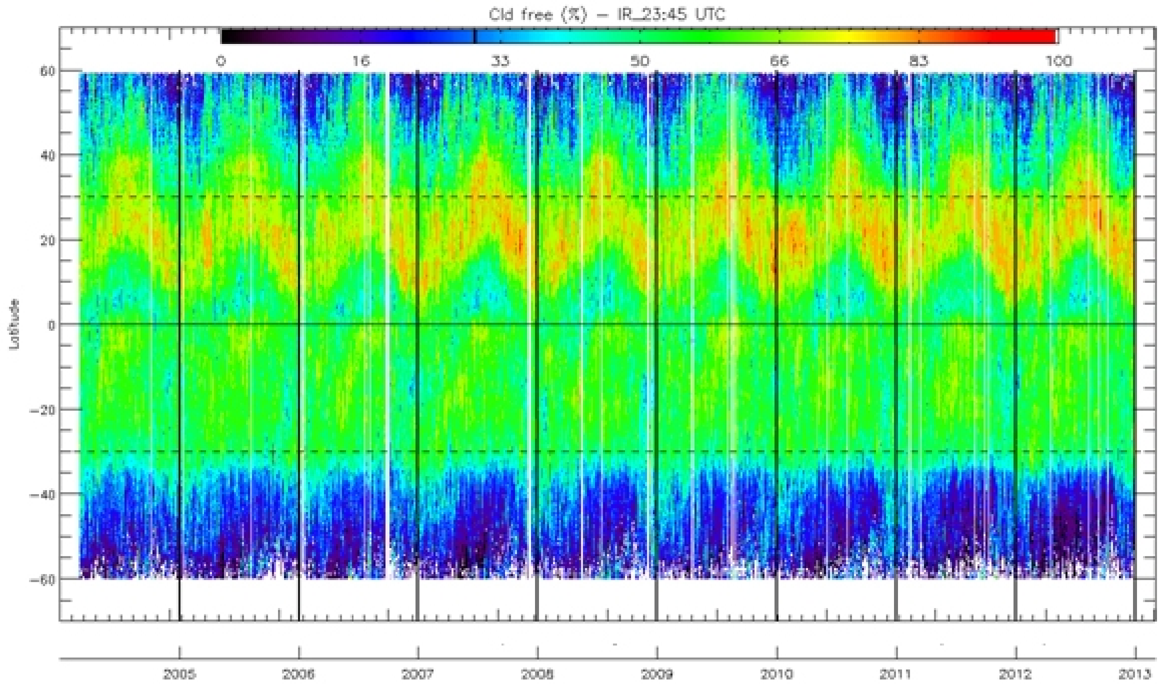

Figure 20: *Clear sky fraction over the period 2004-2012 at 11:45 UTC. Note that CSR is computed only if there is a minimum of 7 clear pixels in the 16x16 pixels box.*

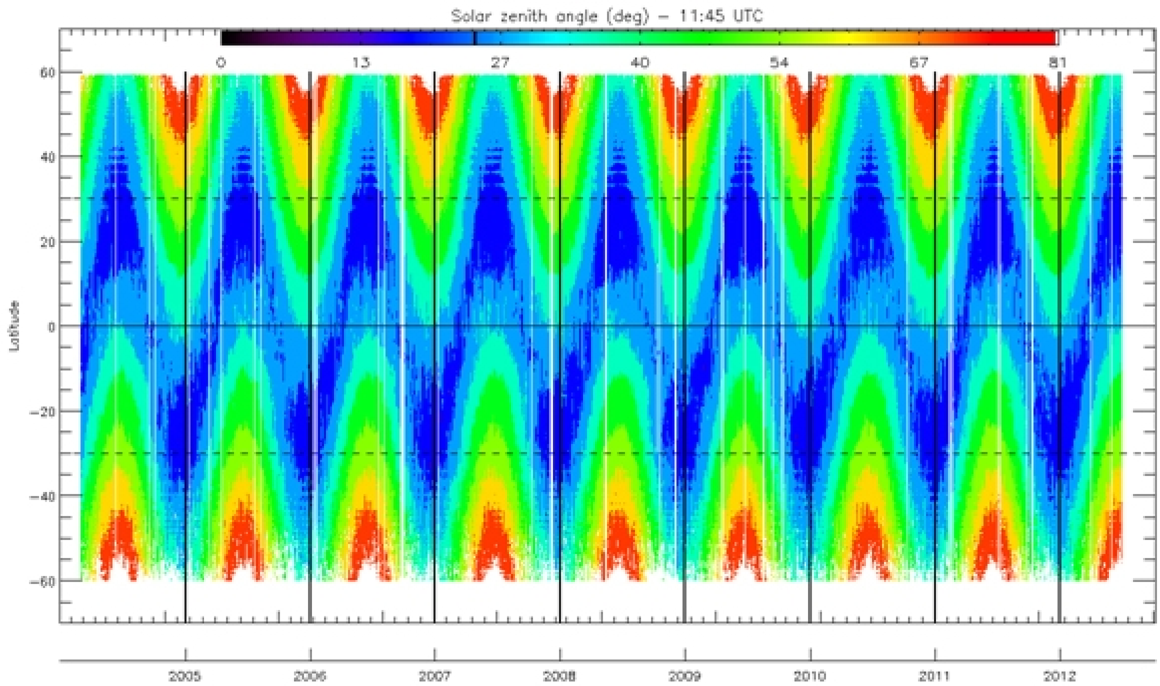

Figure 21: *Solar zenith angle over the reprocessed period 2004-2012 at 11:45 UTC.*

Figure 17 to Figure 19 present the zonally averaged CSR BTs over the 8 year period. The series are stable over the period. The time series exhibits a seasonal cycle of warm temperatures around 20°N and 20°S. The clear sky fraction (in a 16x16 pixel box) is shown on Figure 20. The minimum clear sky fraction is located at latitudes pole-wards of 40°. The maximum clear sky fraction is located in the northern hemisphere. Over the northern hemisphere, a seasonal cycle of clear fraction oscillates between 15 and 40° north and presents a maximum in summer (July, and August) and a minimum in winter. The zonally averaged time series of solar zenith angle at 11:45 UTC, that is also part of the CSR product, is shown on Figure 21

3.3.3 Specific areas

Three desert targets were selected (Figure 22). The Bodélé location, in Chad, was chosen because it is one of the key dust sources in the world. The daily temperature can drop by almost 10°C on a dusty day (see Figure 6 in *Washington et al., 2006*). Those big dust events can probably explain the second minima found every year around September and October (Figure 23c). The two other desert targets Murzuq and Libya are chosen because they are recognised to be very homogeneous bright surfaces. The Libyan site was used for vicarious calibration (*Rao et al., 1999*). Over the 8 year period, the CSR shows a clear annual cycle presenting a maximum in northern hemisphere summer and a minimum in winter. Over desert, the midday temperatures are over 30°C warmer that night-time temperatures. The time series of the brightness temperature sensed by the IR 10.8 µm channel is presented in Figure 23 .

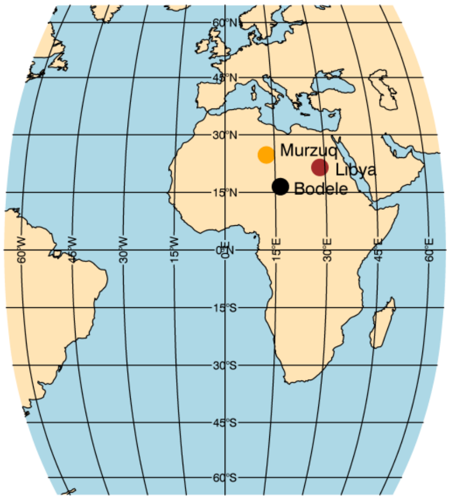

Figure 22: *The three desert targets chosen are Bodélé (lat: 16.5°N, lon 16.5°E), Murzuq (lat: 24.7°N, lon: 12.5°E), and Libya (lat:21.5°N, lon 28.5°E).*

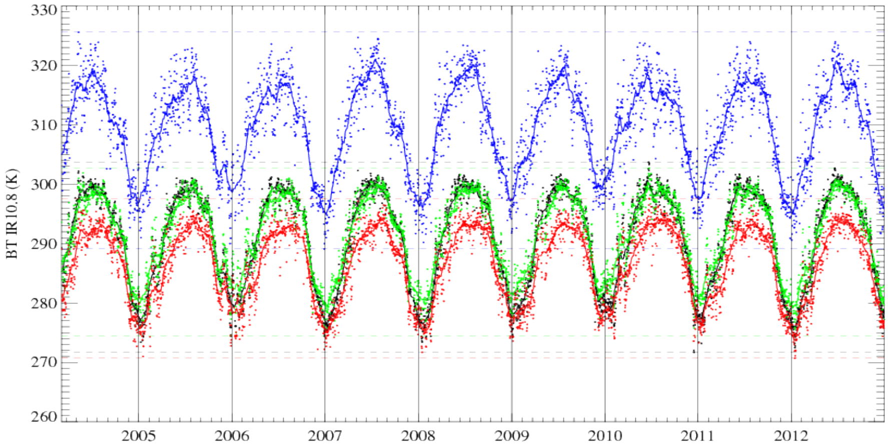

a) Libya

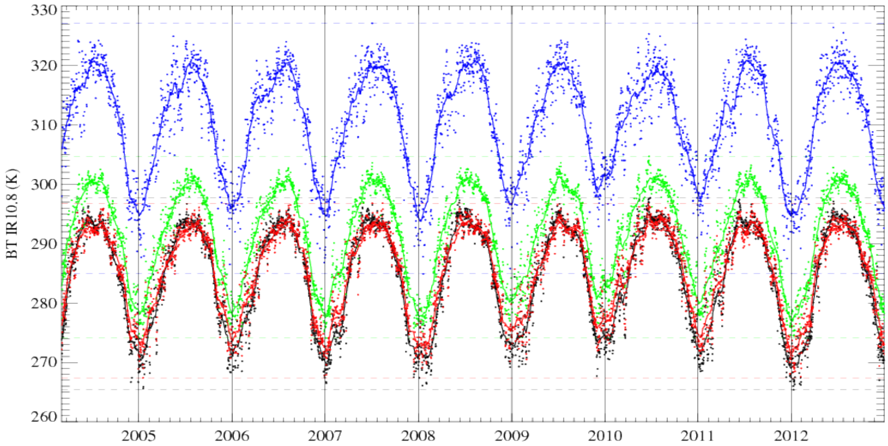

b) Murzuq

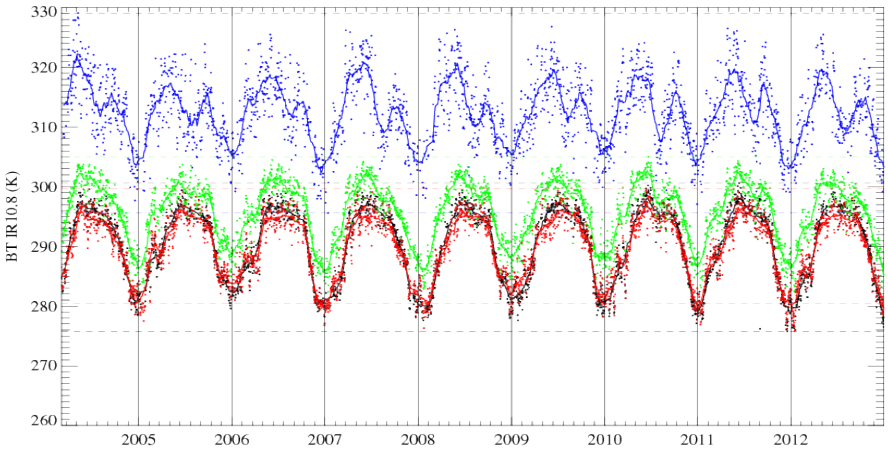

c) Bodélé

Figure 23: *CSR BT for channel 10.8 µm over three desert areas chosen in the MSG disk. The solid lines are the running averages over 30 days at 05:45, 11:45, 17:45 and 23:45 UTC represented in black, blue, green and red, respectively. The coloured dots are the daily measurement at a time.*

In conclusion, the CSR time series over desert are stable and homogeneous.

3.4 Conclusion

The reprocessed CSR slightly differs from the operational product because of the usage of different forecast data as static input. Those ERA interim forecast data are certainly more homogeneous that the one used in MPEF NRT. That has some influence on the cloud detection procedure and consequently on the retrieved cloud free temperatures. The average difference is below 0.1 K. The 8-year time series is very stable and does not exhibit any significant trends on desert targets.

4 ALL SKY RADIANCES

4.1 Product definition

The All Sky Radiances (ASR) product contains information on mean brightness temperatures from all thermal (e.g. infrared window and water vapour) channels [RD2]. The ASR product is produced by averaging SEVIRI thermal channel brightness temperatures over a certain image section defined as a box (Field of Regard - FoR) of 16 by 16 image pixels. Spatial resolution of SEVIRI thermal channels is 3 km by 3 km and therefore the FoR resolution is 48 km by 48 km close to the centre of SEVIRI image. ASR is generated by MPEF hourly in NRT. The product has only been reprocessed three hourly [RD2].

4.2 Comparison with operational products

A check against the operational product is shown for a particular month only (Table 5). For all channels, the bias between RMPEF and MPEF products is negligible (below 0.01 K). This is because the images used to reprocess the ASR product are the same as the operational images used in NRT. There is no cloud mask used for the ASR product generation, resulting in negligible differences between the MPEF and RMPEF corresponding products. Few differences appear over Africa where the RMPEF ASR pixels are slightly colder than the corresponding MPEF ASR one (see Figure 24 and Figure 25). This very small difference is even smaller at nighttimes (see Table 3 of *RD3*).

Channel	Average (K)	Std dev (K)	Bias (K)	Rms (K)
BT 12	**283.1** (283.1)	**10.2** (10.2)	-0.01	0.27
BT 108	**284.6** (284.6)	**20.1** (20.1)	-0.01	0.25
BT 96	**261.2** (261.2)	**14.7** (14.7)	-0.01	0.15
BT 87	**282.6** (282.6)	**18.4** (18.4)	-0.01	0.21
BT 73	**256.8** (256.8)	**11.3** (11.3)	-0.00	0.06
BT 62	**239.9** (239.9)	**9.2** (9.2)	0.00	0.06
BT 39	**291.8** (291.8)	**16.5** (16.5)	-0.01	0.19

Table 5: *Statistics for the month of June 2008 at 11:45 UTC showing the differences between the RMPEF and the MPEF ASR products. Bold values are reprocessed values and values in brackets are for the operational products. Bias = RMPEF-MPEF.*

BT10.8, June 2008 at 11:45

A) Monthly average of RMPEF ASR (K) and difference (K) of the average RMPEF-MPEF

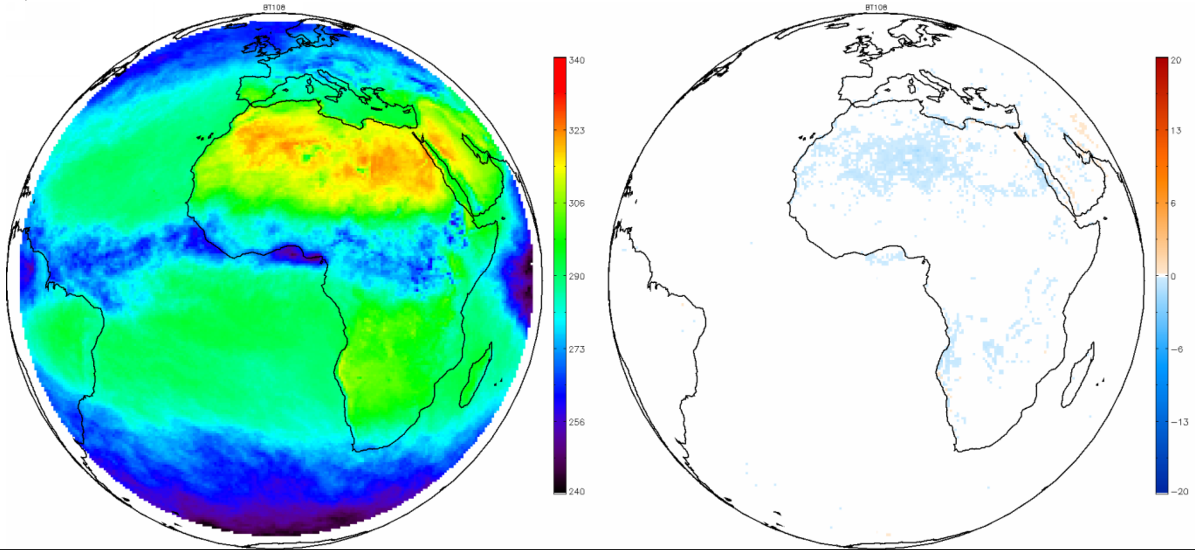

b)

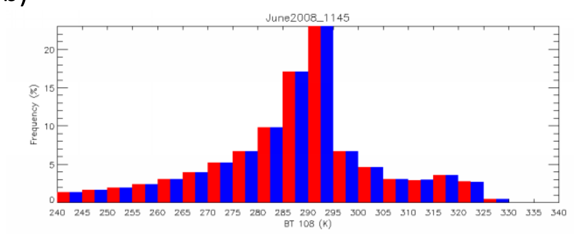

c)

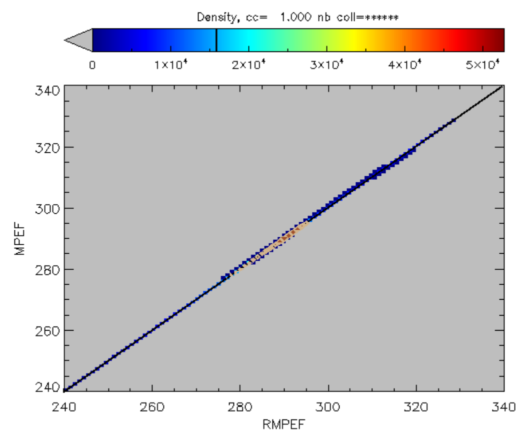

Figure 24: *a) Average of the RMPEF ASR BT for SEVIRI channel IR10.8 and difference avg(RMPEF)-avg(MPEF), b) histogram of the RMPEF BT in red and the MPEF (in blue), and c) scatter plot of MPEF BT as a function of RMPEF ASR for the SEVIRI channel centred at 10.8 μm.*

BT7.3, June 2008 at 11:45

A) Monthly average of RMPEF ASR (K) and difference (K) of the average RMPEF-MPEF

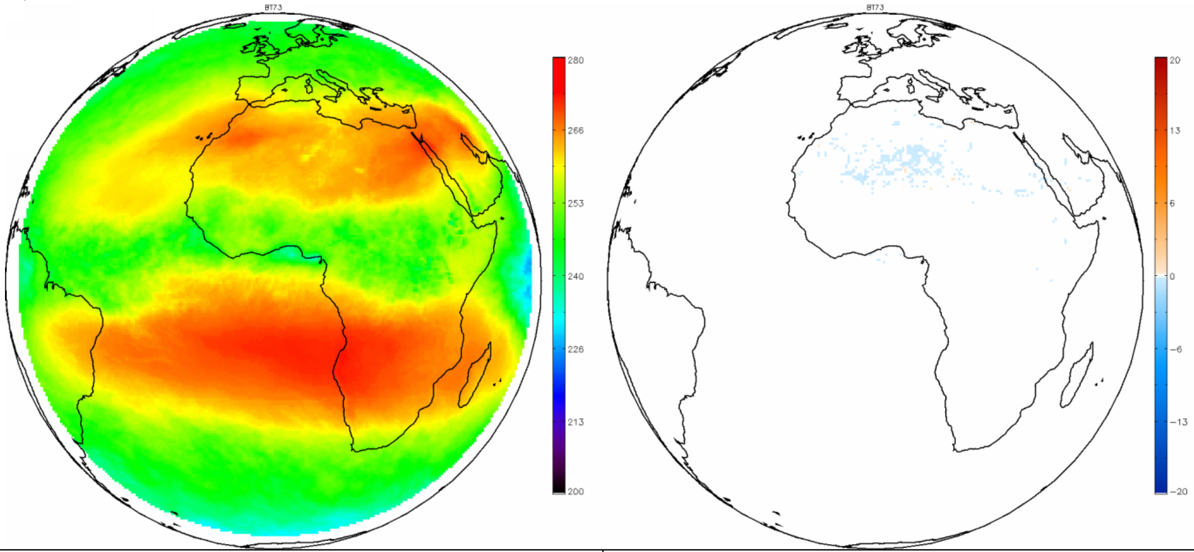

b)

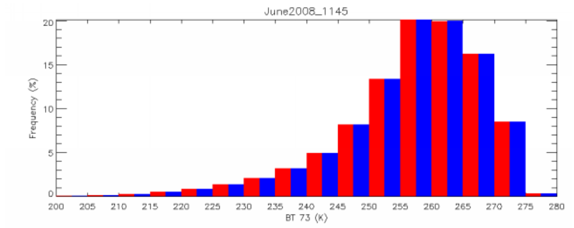

c)

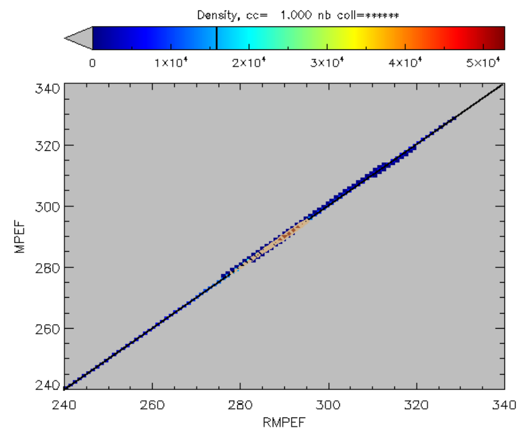

Figure 25: *Same as Figure 24 but for the SEVIRI channel centred at 7.3 µm.*

4.3 Temporal stability

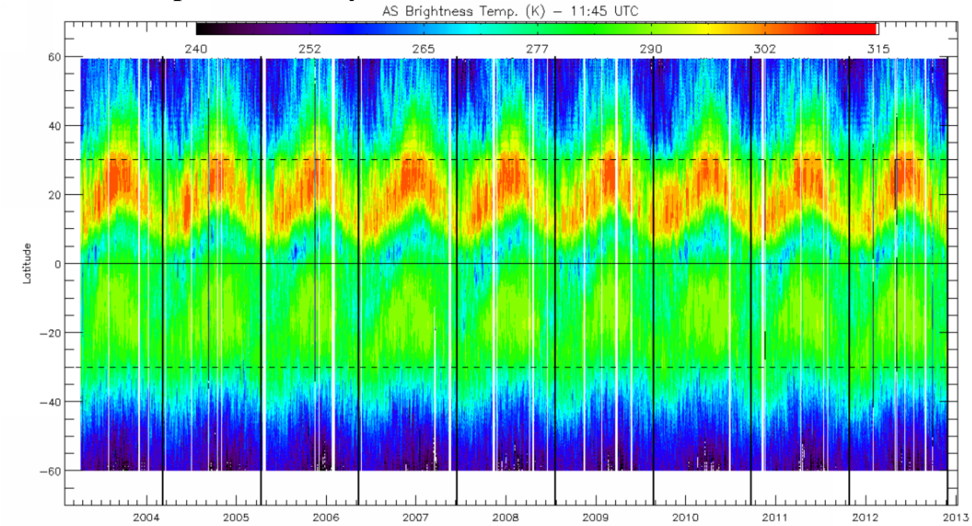

a) ASR in channel 9 (10.8 µm) at 11:45 UTC

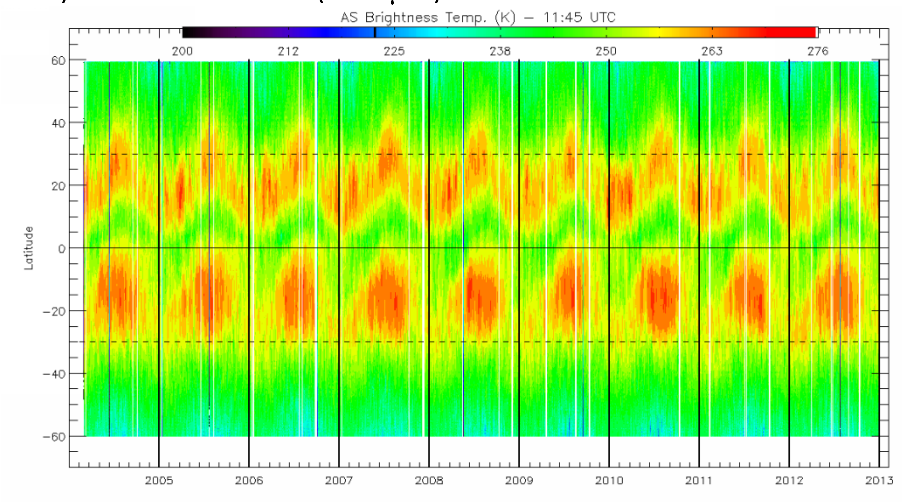

b) ASR in channel 6 (7.3 µm) at 11:45 UTC

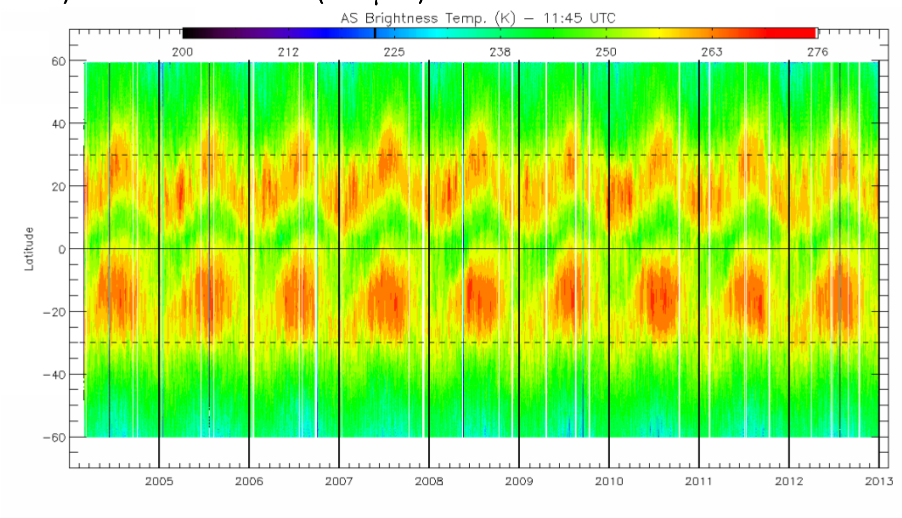

c) ASR in channel 5 (6.2 µm) at 11:45 UTC

Figure 26: *ASR (K) over the eight year period at 11:45 UTC for 3 different channels.*

The time series is very stable over the 8-year period as shown on Figure 26. Every channel presents a warm BT around 20° north and south. A seasonal cycle appears with a warm temperature in northern hemisphere summer and cold temperatures in southern hemisphere winter.

4.4 Comparison with other dataset

Hyper-spectral infrared sounders such as the Atmospheric InfraRed Sounders (AIRS) and the Infrared Atmospheric Sounding Interferometer (IASI) are generally used to calibrate or validate broadband channel radiances/brightness temperatures [*Hewison et al., 2013*]. AIRS is not considered here because it has a local overpass time of ~1:30 AM/PM and therefore 90 minutes apart from ASR sampling time. The local overpass time of IASI is ~9:30 AM/PM, and thus there is a certain probability for the measurements to be close in time with ASR data. We have taken IASI data from the Global Space-based Inter Calibration System (GSICS) server (http://gsics.eumetsat.int/thredds/catalog/metopa-iasi/catalog.html) for 2010-2012. These data are used to inter-calibrate MSG SEVIRI radiances with IASI. Note that the corrections based on the inter-calibration were not applied while deriving the products considered here. GSICS used only night time data and the orbit which passes closest to the centre of the MSG image. Figure 27 shows the distribution of the start time of the IASI files and most of the retrievals in these files are measured after 9 PM. There are only 9 files which have starting acquisition time matching the ASR data: 3 from January 2010 and 6 from December 2012.

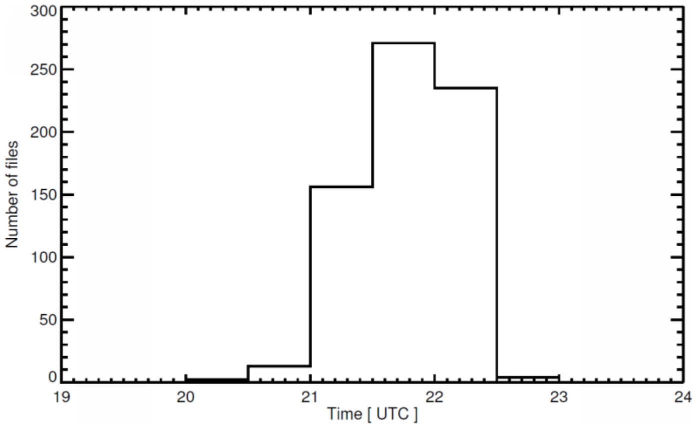

Figure 27: *Distribution of start time of GSICS IASI files.*

To collocate IASI radiances with ASR data, we have first gridded both data to a common grid. The grid size is selected in such a way that one grid box contains only one ASR measurement whose size is approximately 48 km by 48 km. The footprint size of an IASI pixel is 12 km by 12 km (see, for example, Figure 4.3 of http://oiswww.eumetsat.org/WEBOPS/eps-pg/IASI-L1/IASIL1-PG-4ProdOverview.htm) and therefore there can be 2 to 4 IASI pixels in a grid box. This method is significantly faster than the conventional distance calculation method. IASI spectral radiances are first converted to brightess temperatures to be compared with SEVIRI ASR BT. These spectra in brightness temperatures are then convolved with spectral response functions (SRF) of SEVIRI channels to mimic brightness temperatures as they would have been measured by SEVIRI. At each grid box, we computed the mean and the standard deviation of the pseudo SEVIRI brightness temperatures computed from IASI spectra. It has to be noted that the correct method of computing brightness temperatures from IASI should be to first compute average radiances and then to convert them to brightness temperatures. However, we averaged brightness temperatures to match the procedure used in ASR.

Stringent collocation criteria are used to obtain robust results: the maximum time difference allowed is 5 minutes and the maximum zenith angle difference (max_{θ}) allowed is 0.05° with $max_{\theta} = \left|\left(\frac{\cos\vartheta_{ASR}}{\cos\vartheta_{IAS}}\right) - 1\right|$, which is consistent with GSICS criteria. However, we have also tested a time threshold of 10 minutes which can be justified due the higher spatial averaging of ASR compared to the pixel level (i.e., 3 km by 3 km) collocation by GSICS (provide results of sensitivity analyses). Therefore we have also given statistics based on match up data with 10 minutes threshold which are provided in brackets immediately after statistics based on match up data with 5 minutes threshold.

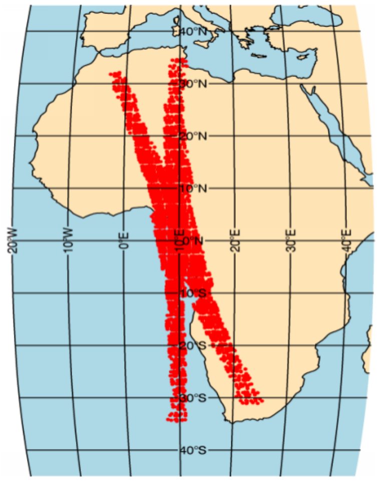

Figure 28: *Locations of IASI pixels matching with ASR data for the 9 IASI overpasses (see text for details).*

After filtering, 4659 (8501) collocations remain (Figure 28) which are shown in Figure 29 (collocations using 10 minutes threshold are not shown) for 3 channels: 6.2 µm channel which is sensitive to the upper tropospheric relative humidity, 7.3 µm channel which is sensitive to the mid tropospheric relative humidity and 10.8 µm channel which is a window channel senstive to the surface and/or cloud emission.

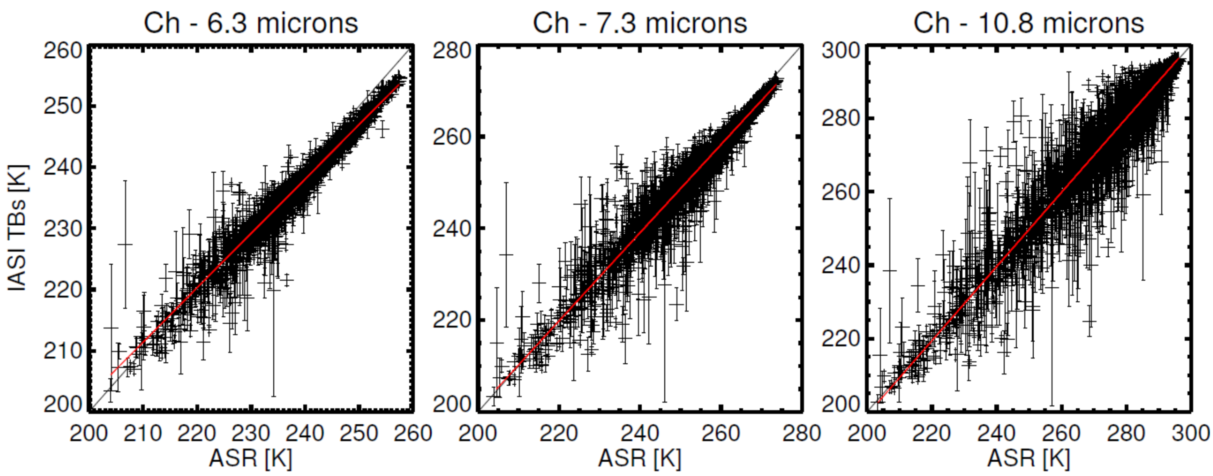

Figure 29: *Collocated ASR and average IASI brightness temperatures within each ASR. Error bars denote the standard deviation of IASI brightness temperatures within one ASR measurement divided by square root of number of IASI pixels. An offset of 0.3K is added to the standard deviation of IASI brightness temperatures to account for the radiometric noise of SEVIRI measurements.*

	Bias [K]	RMSD [K]	Correlation	Slope [K/K]
Ch 6.3	1.91 (1.97)	2.33 (2.35)	0.976 (0.979)	0.889 (0.902)
Ch 7.3	1.73 (1.69)	2.77 (2.68)	0.974 (0.974)	0.962 (0.967)
Ch 10.8	-0.08 (0.10)	4.00 (3.87)	0.969 (0.964)	1.010 (1.001)

Table 6: *Statistics of collocated ASR and IASI measurements. Values shown are for 5 minutes collocation threshold and 10 minutes collocation threshold, which are in brackets.*

ASRs for the two water vapour channels show a warm bias especially for clear sky and dry scenes.

Note that the bias and linear fit are computed as weighted statistics, for example, bias is defined as:

$$bias = \frac{\sum_{i=0}^{n} (ASR_{MSG} - BT_{IASI})_i std_i^{-2}}{\sum_{i=0}^{n} std_i^{-2}}$$

where std_i is the standard deviation of IASI BT for the i^{th} collocation.

4.5 Conclusion

There is almost no difference between the reprocessed and the operational ASR data. The benefit of the reprocessing for the ASR product is small as there is little added value to the NRT product (neither change in the retrieval scheme nor in the input images). It has to be noted that ASR are available from the EUMETSAT archive only since June 2008, the reprocessing enable the user to have access to ASR data for the entire 8-years period. The first ever comparison between MSG ASR products and IASI brightness temperature indicates that the MSG ASR shows a warm bias in the water vapour channels for rather clear sky and dry scenes

5 CONCLUSIONS

The complete MSG time series has been reprocessed for the period March 2004 until December 2012. The three level-2 products, AMV, CSR, and ASR, validated in this document, were shown to be very stable over the eight-year period. This gives some confidence in their climatological quality and their suitability to be assimilated into the ECMWF forecast model for reanalysis. The validity of this dataset has been proven by the comparison with collocated external dataset.

The main benefits of the reprocessing of the EUMETSAT geostationary products are:

- The same algorithm was used over the entire period,
- The reprocessed level-2 products are stable temporally and can be used for climate studies. Trends may not be computed because the reprocessed time series is relatively short (only 8 years) and the stability has not been assessed in absolute terms.

The reprocessing of MSG level-2 product has been especially valuable for AMVs because it has led to a complete stable and homogeneous time series over the period. The benefit of the reprocessing is less clear for the CSR and ASR products that look very similar to the operational NRT products. The operational ASR are not available prior to 2008. For ASR, the benefit of the reprocessing exercise is to get them over the entire 8-years MSG period.

The next Release of MSG reprocessed products will be produced using SEVIRI images recalibrated to IASI data. Under those conditions the CSR and ASR reprocessed products are expected to be significantly superior to the NRT products.

6 SCIENTIFIC BIBLIOGRAPHY

- Borde, R., M. Doutriaux-Boucher, G. Dew, M. Carranza, (2014), A direct link between feature tracking and height assignment of operational EUMETSAT Atmospheric Motion Vectors. *J. Atmos. Oceanic Technol.*, **31**, 33–46. doi:10.1175/JTECH-D-13-00126.1.

- Borde, R., (2010), AMV improvements, proceeding from 10th International WindWorkshop.

- Carranza M., A. De Smet, M. Doutriaux-Boucher, R. Borde, and G. Dew, (2012), Long-term Statistics of MSG winds, proceeding *of the 11th International Wind Workshop*, Auckland, New-Zeland, 20-24 Feb 2012.

- Dee et al. (2011), The ERA-Interim reanalysis, configuration and performance of the data assimilation system, *Q. J. R. Meteorol. Soc.,* **137**, 553-597.

- Doutriaux-Boucher M., M. Forsythe, R. Saunders and P. Francis, MSG wind height assignment problems, *Met Office technical note 469*, 2006.

- García-Pereda, J. and R. Borde (2014), The Impact of the Tracer Size and the Temporal Gap between Images in the Extraction of Atmospheric Motion Vectors. *J. Atmos. Oceanic Technol.*, **31**, 1761–1770.

- Haimberger, L., C. Tavolato, and S. Sperka, (2012), Homogenization of the global radiosonde temperature tataset through combined comparison with reanalysis background series and neighbouring Stations, *J. Climate*, **25**, 8108-8131.

- Hamann et al., (2014), Remote sensing of cloud top pressure/height from SEVIRI: analysis of ten current retrieval algorithms, *Atmos. Meas. Tech*., 7, 2839-2867.

- Hewison, T. J., X. Wu, F. Yu, Y. Tahara, X. Hu, D. Kim and M. Koenig (2013), GSICS Inter-Calibration of Infrared Channels of Geostationary Imagers using Metop/IASI, *IEEE Trans. Geosci. Remote Sens.*, **51**, 3, doi:10.1109/TGRS.2013.2238544.

- Holmlund K., C. S. Velden, (1998), Objective determination of the reliability of satellite derived Atmospheric Motion Vectors, *Proceedings of the 4th International Wind Workshop*, Saanenmöser, Switzerland, 20-23 October 1998.

- Holmund K., C. S. Velden, M. Rohn, (2001), Enhanced automated quality control applied to high-density satellite-derived winds, *Mon. Wea. Rev.,* **129**, 517-529.

- Huffman, G.J., D.T. Bolvin, R.F. Adler, last updated 2012, GPCP Version 2.2 SG Combined Precipitation Data Set. WDC-A, NCDC, Ashville, NC, 2012. http://www.ncdc.noaa.gov/oa/wmo/wdcamet-ncdc.html.

- GCOS 154, Systematic observation requirements for satellite-based data products for climate, (2011 update), Supplemental details to the satellite-based component of the

Implementation Plan for the Global Observing System for Climate in Support of the UNFCCC.
http://www.wmo.int/pages/prog/gcos/documents/SatelliteSupplement2011Update.pdf

- Munro R., C. Köpken, G. Kelly, J.-N. Thépaut and R. Saunders, (2004), Assimilation of Meteosat radiance data within the 4D-Var system at ECMWF: Data quality monitoring, bias correction and single-cycle experiments, *Q. J. R. Meteorol. Soc.,* **130**, pp. 2293–2313.

- Nieman,S.J., W. P. Menzel, C. M. Hayden, D. Gray, S. T. Wanzong, C. S. Velden, and J. Daniels, (1997), Fully automated cloud-drift winds in NESDIS operations, *Bull. Amer. Meteor. Soc.,* **78**, 1121-1133.

- Rao, C.R. N., J. Chen, J. T. Sullivan, and N. Zhang, (1999), Post-launch Calibration of Meteorological Satellite Sensors, *Advances in Space Research*, **23**, 1357-1365

- Rohn, M., G. Kelly, and R. W. Saunders (2001), Impact of a new cloud motion wind product from Meteosat on NWP analyses and forecasts, *Mon. Wea. Rev.*, 129, 2392-2403.

- Washington, R., M. C. Todd, S. Engelstaedter, S. Mbainayel, and F. Mitchell (2006), Dust and the low-level circulation over the Bodélé Depression, Chad: Observations from BoDEx 2005, *J. Geophys. Res.*, **111**, D03201, doi:10.1029/2005JD006502.

- Szyndel, M. D. E., G. Kelly, and J.-N. Thépaut (2005), Evaluation of potential benefit of assimilation of SEVIRI water vapour radiance data from Meteosat-8 into global numerical weather prediction analyses, *Atmos. Sci. Lett.*, **6**, 105–111.